LAWRENCE
LIVERMORE
NATIONAL
LABORATORY

UCRL-AR-217329

Evaluation of the NARAC Modeling System. Final Report to the Lawrence Livermore National Laboratory

Jeffrey C. Weil

November 29, 2005

This work was performed under the auspices of the U.S. Department of Energy by University of California, Lawrence Livermore National Laboratory under Contract W-7405-Eng-48.

Evaluation of the NARAC Modeling System

Final Report to the
Lawrence Livermore National Laboratory
Livermore, CA

Jeffrey C. Weil

Cooperative Institute for Research in Environmental Sciences
University of Colorado, Boulder, CO 80309

September 30, 2004

1. Introduction

Dispersion of hazardous material in the planetary boundary layer (PBL) occurs as a result of the turbulent air motion within that layer. PBL turbulence is driven by the surface heat and momentum fluxes and is damped by stable stratification, which can exist either within the layer (stable PBL) or above the layer (convective and stable PBLs). The daytime PBL is typically 1 to 2 km deep depth whereas its nighttime counterpart may range from a few 10s of meters to a few 100 m. Dispersion varies widely depending on the source conditions (height, duration, buoyancy, etc), the mean wind and turbulence fields, the PBL depth, and the surrounding terrain. Atmospheric dispersion models simulate or parameterize the above features in a variety of ways to predict the concentration field downwind of a source.

Releases of hazardous and toxic materials in an emergency response pose unique challenges since the releases may come from instantaneous, short-duration, or continuous releases of unknown strength and location and the meteorology may be ill-defined. Despite these challenges, emergency response models are necessary to assist in the planning of an evacuation and to be run in "real" time to forecast the transport, dispersion, and concentration field of a hazardous cloud. One such modeling system is the Department of Energy's National Atmospheric Release Advisory Center (NARAC) system.

Given the reliance on models, it is necessary to know their accuracy and limitations. Model evaluation is an important activity and generally has proceeded by: 1) assessing the model physics, 2) determining the model's "operational performance", and 3) distinguishing the difference in performance between two or more models (Weil et al., 1992). A model physics evaluation addresses whether or not a model gives good predictions for the "right" reasons. In contrast, an operational performance evaluation may merely determine the overall bias of a model and if it correctly predicts the magnitude of the highest concentrations regardless of the actual conditions producing them.

The purposes of this report are: 1) to give a brief overview of the NARAC model, 2) to describe the databases used in evaluating the model, and 3) to present an evaluation of NARAC, where emphasis has been on the the transport and dispersion components. The evaluation covers both the model physics and operational performance of NARAC.

2. The NARAC Dispersion Model

The NARAC model addresses the transport and dispersion of hazardous and toxic materials from instantaneous, short-duration, and continuous sources. The emissions may consist of gases, liquid droplets, and solid particles. In addition, the model accounts for the effects of source buoyancy and momentum, chemical and physical transformations, gravitational settling of particles, and wet and dry deposition. The NARAC model consists of a transport and dispersion component, the Lagrangian Operational Dispersion Integrator (LODI), coupled with a meteorological data assimilation model, the Atmospheric Data Assimilation and Parameterization Tool (ADAPT), for providing the wind field (Nasstrom et al., 2000; Sugiyama and Chan, 1998; Sugiyama et al., 2002).

In the following, we give a brief overview of the transport and dispersion formulation including the treatment of source buoyancy and momentum.

2.1. Dispersion and Concentrations

LODI uses the three-dimensional (3-D) diffusion equation as its basis. The turbulent dispersion is solved with a Lagrangian stochastic particle model with advection by the mean wind provided by ADAPT. For a passive scalar, the diffusion equation is given by the general form

$$\frac{\partial C}{\partial t} + \overline{u}_i \frac{\partial C}{\partial x_i} = \frac{\partial}{\partial x_i}\left(K_{ij}\frac{\partial C}{\partial x_j}\right) \ , \tag{2.1}$$

where C is the mean concentration (over a large ensemble of realizations), $\overline{u}_i$ is the mean wind in the ith direction at point $x,\ y,\ z$, K_{ij} is the eddy diffusivity tensor, and t is time. In LODI, it is assumed that the diffusivity tensor is diagonal or that K_x, K_y, and K_z (where $K_x = K_{xx}$, etc.) are the only nonzero components. Other terms are added to Eq. (2.1) to describe the effects of gravitational settling, chemical decay, and physical transformations.

As discussed by Durbin (1983), an eddy-diffusion (K) model is a stochastic model for particle displacements in a Lagrangian framework. The K-model concept is applicable in the case of a vanishingly small Lagrangian integral time scale T_L or when $t \gg T_L$ such that one need not consider T_L explicitly. In essence, this is what is assumed in LODI. The general equation for the infinitesimal particle displacement dx_{pi} in the ith direction is given by the stochastic differential equation (e.g., see Rodean, 1996)

$$dx_{pi} = \overline{u}_i dt + \frac{\partial K_{ij}}{\partial x_j}dt + (2K_{ij})^{1/2} d\xi_j \ , \tag{2.2}$$

where $d\xi_j$ is the jth component of an independent Gaussian random process. In LODI, it is assumed that the turbulence is homogeneous in the horizontal directions, x and y, such that $\partial K_x/\partial x$ and $\partial K_y/\partial y$ are zero. The only turbulence inhomogeneity considered is in the vertical direction z so that $\partial K_z/\partial z$ can be nonzero.

There are a number of options for specifying the eddy diffusivities in the stochastic model. For the vertical diffusivity, two simple possibilities are given primarily for testing the model against analytical solutions for the concentration: 1) a constant K_z (user specified), and 2) a power law form for K_z. The constant K_z in combination with a uniform wind speed should produce a Gaussian distribution of C with z (Pasquill and Smith, 1983), and the power law form of K_z also yields analytical solutions (Smith, 1957; Nieuwstadt, 1980). A third option which is probably the most useful for atmospheric applications is a K_z for the entire boundary layer ($z < z_i$) (Lange, 1989)

$$K_z = \frac{k u_* (z - z_g)}{\phi_h} \exp\left(\frac{-c_k (z - z_g)}{z_i}\right) \ , \tag{2.3}$$

where k is the von Karman constant ($= 0.4$), u_* is the friction velocity, z is height above a reference level, z_g is the local surface height above the reference level, ϕ_h is the Monin-Obukhov (MO) dimensionless temperature gradient, c_k is a constant ($= 4$), and z_i is the boundary layer height. The term preceeding the exponential function is the K_z for the surface layer.

The K_z formulation could be made more general by incorporating a term to account for the convective boundary layer (CBL) turbulence, i.e., a term $\propto w_* z_i$, where w_* is the convective velocity scale; e.g., see Holtslag and Moeng (1991). However, the eddy diffusion concept used in LODI does not apply in principle to vertical dispersion from an elevated source in the CBL due to the existence of large eddies with large Lagrangian integral timescales, $T_L \propto z_i/w_*$ (Lamb, 1982; Weil, 1988a), and hence with velocities correlated over times $\sim T_L$. In contrast, K theory is based on a zero or vanishingly small T_L.

For the horizontal diffusivities, it is assumed that $K_x = K_y$. As with the vertical component, there is an option for a constant $K_x,\ K_y = K_H$, which is user specified. The main form for specifying the diffusivity K_y uses the large-time limit ($t \gg T_L$) of statistical theory: $\sigma_y^2 = 2\sigma_v^2 T_L t$ (Taylor, 1921), wherein the diffusivity is $K_y = \sigma_v^2 T_L$. This form is applicable for stationary homogeneous turbulence, conditions which are assumed to apply in the horizontal directions. For a semi-empirical relationship in which σ_y versus t may be more general, the "effective" diffusivity can be defined as $K_y = (1/2)(d\sigma_y^2/dt)$ (Csanady, 1973; Pasquill and Smith, 1983). LODI uses this effective formulation together with Draxler's (1976) form for σ_y to determine the K_y.

Draxler's σ_y expression is given by

$$\sigma_y = \sigma_v t f_D \ , \tag{2.4a}$$

where

$$f_D = \frac{1}{1 + 0.9(t/T_D)^{1/2}} \ , \tag{2.4b}$$

and T_D is an empirical time scale. The T_D, defined as the time at which $f_D = 0.5$, is related to T_L as found by Draxler (1976), $T_D = 1.64 T_L$. Draxler recommended a $T_D = 1000$ s for lateral dispersion from an elevated source in unstable conditions, i.e., the CBL. In LODI, the T_D parameterization for the CBL is given by

$$T_D = \frac{z_i}{(27u_*^3 + 1.2w_*^3)^{1/3}} \ , \tag{2.5}$$

which is based on the work of Briggs (1985) and Nieuwstadt and van Duuren (1978). Draxler (1976) found that his model was valid in all cases of lateral dispersion. However, for vertical dispersion, he found the model to be inapplicable for: 1) a surface source in unstable conditions, and 2) an elevated source in stable conditions. In both cases, the inapplicability was due to the vertical inhomogeneity of the turbulence. Note that Draxler's vertical dispersion parameterization is not used in LODI.

As this discussion suggests, the diffusion equation approach with dispersion solved by a Lagrangian particle displacement model is most applicable to dispersion from near-surface sources where the T_L is small. It also may be useful for elevated sources in a stable environment, when the T_L is small compared to travel times of interest. The approach is most questionable in the case of elevated sources in the CBL, which has a large T_L. These features are recognized by the LODI developers (e.g., see Ermak and Nasstrom, 2000) who also considered the key requirement of computational speed in formulating LODI. For dispersion, the Lagrangian displacement model used in LODI is computationally faster than solving a Lagrangian stochastic model for particle velocities (e.g., Rodean, 1996; Weil, 1990) with subsequent time integration to obtain the particle displacements.

In summary, the Lagrangian displacement model used in LODI is a reasonable and practical approach for a number of atmospheric dispersion problems. A key issue is the applicability and accuracy of this approach for elevated passive and/or buoyant releases in the CBL. The current evaluation addresses elevated passive releases (Section 4).

2.2. Source Buoyancy and Momentum Effects

Plume rise is obtained from an integral approach based on equations governing the total fluxes of mass, momentum, and energy through a plume cross section. The basic assumptions such as the Boussinesq approximation regarding density differences between the plume and environment and "top hat" profiles of plume properties over the cross section are standard for integral plume models (Briggs, 1975; Weil, 1988b). The key closure assumption is that the entrainment of ambient air by the plume is proportional to the plume vertical velocity times the plume radius; the entrainment is controlled by plume-generated turbulence. These assumptions lead to analytical solutions for the plume rise and radius in a neutral or unstratified environment in the case where ambient turbulence is neglected (Briggs, 1975; Weil, 1988b); for a buoyant plume, the rise $\Delta z_r(t) \propto t^{2/3}$, and for a momentum-dominated plume, $\Delta z_r(t) \propto t^{1/3}$.

In the PBL, the plume rise can be limited by 1) ambient turbulence, 2) stable stratification with a uniform potential temperature gradient, or 3) an elevated stable layer capping a well-mixed, zero potential temperature gradient region, i.e., the mixed layer. In LODI, the final rise due to each of these effects is computed separately and the minimum final rise is adopted. In addition, for sources with both initial momentum and buoyancy, the final rise is computed separately for each source term and the higher of the two final rises is chosen.

3. Copenhagen and OLAD Field Data

3.1. Copenhagen Experiment

The Copenhagen experiment consisted of eleven 1-h SF_6 tracer releases conducted during 1978 and 1979 (Gryning and Lyck, 1984). The releases were nonbuoyant and were made from a height of 115 m on a TV tower in a northern residential area of Copenhagen. The terrain was relatively flat and the monitors were placed at $\sim 2^\circ$ intervals on three approximately radial arcs at distances of 2, 4, and 6 km downwind; about 20 monitors were located on each arc. The downwind sector chosen for the experiments was determined by the availability of roads and by avoiding special topographical features that would affect the dispersion process. The upwind sector included some industrial areas approximately 3 km from the tower but overall was characterized as residential. The downwind sector was residential except for a mixed park-forest complex to the northeast about 7 km from the tower. Based on vertical wind variances and mean wind profiles, the roughness length was estimated to be about 0.6 m.

The experiments were carried out during daytime under near-neutral to convective conditions with the stability index $-z_i/L$ ranging from 1.4 to 43; here, L is the MO length (Eq. 4.1). Most ($\sim 90\%$) of the values fell in the range $1.4 \leq -z_i/L \leq 14$, which could be labeled as weakly-to-moderately convective turbulence; see Section 4. Wind speed, wind direction, and temperature were measured at heights ranging from 2 m to 120 m, and

turbulence measurements were obtained at the 115-m level on the tower.

3.2. Overland Along-Wind Dispersion (OLAD) Experiment

The OLAD field experiment was conducted in September 1997 at the West Desert Test Center of the U.S. Army Dugway Proving Ground in Utah (see Chang et al., 2003). The test domain was mostly a dry mud flat with surrounding mountains, and the typical z_0 in the broad valley was 3 cm. The experiment involved line releases of SF_6 from a truck or airplane in the early morning hours with a predominant wind direction from the southeast. The truck releases were made over a distance of 8 km and at a height of 3 m above ground, whereas the airplane releases were made over a distance of 16 km and at 100 m above ground. Eleven separate releases were conducted between 3 AM and 9:45 AM with most of them between 5:45 AM and 7 AM and typically during stable or near-neutral conditions. Three sampling lines were deployed with 15 samplers per line at a spacing of 100 m; the samplers obtained 15-min averaged concentrations over a total sampling time of 3 h. The lines were located 2, 5, and 10 km downwind of the truck releases and 10, 15, and 20 km downwind of the aircraft releases.

Surface winds were measured by anemometers on eight 2-m masts and eight 10-m towers, and upper-air winds were measured by pibals and radiosondes. The OLAD data were not used in this evaluation but may be used in the future.

4. Evaluation of NARAC with the Copenhagen Data

Evaluation of the NARAC model focused on the performance of its dispersion component LODI for an elevated source in the CBL. LODI was examined in its "baseline" form as described in the LODI User's Guide (Section 4.2), and the LODI σ_y formulation was investigated for its sensitivity to the Draxler time scale (T_D) and the modeled wind profile (Section 4.3). Before presenting the evaluations, we briefly discuss the stability characterization of the CBL.

4.1. CBL Stability Characterization

In the CBL, the stability is categorized by the index $-z_i/L$ (Deardorff, 1972), where L is the MO length

$$L = \frac{-u_*^3 T_o}{kg\overline{w\theta}_o} \ , \tag{4.1}$$

T_o is the mean absolute temperature, and $\overline{w\theta}_o$ is the surface heat flux. The index is the ratio of depths, z_i and $|L|$, over which convective- and shear-generated turbulence, respectively, are important (see Deardorff, 1972; Weil, 1988a). A large value of the index indicates a relatively thin surface shear layer or friction layer, and hence, a CBL dominated by convection.

The CBL turbulence is a continuous function of $-z_i/L$, but it is useful to categorize the turbulence structure and dispersion in broad groups based on $-z_i/L$ as discussed below. In strong convection, the CBL has an approximate triple-layer structure consisting of a surface layer ($z \leq 0.1z_i$), a mixed layer ($0.1z_i \leq z \leq 0.8z_i$), and an interfacial layer

($0.8z_i \leq z \leq 1.2z_i$) (see Wyngaard, 1988). Strong convection exists when $-z_i/L > 20$ (Hicks, 1985), but the above triple-layer structure is most applicable when $-z_i/L > 50$ to 100 (Caughey, 1982); in this case, the surface friction layer ($z < -L$) is quite thin. In moderate convection ($5 \leq -z_i/L \leq 20$), wind shear becomes more important particularly in the surface layer, and it is even more important in weak convection ($0 \leq -z_i/L \leq 5$).

For nine of the ten Copenhagen experiments, $-z_i/L$ was in the range $1.4 \leq -z_i/L \leq 14$, which we consider as weak-to-moderate convection and in one experiment, $-z_i/L = 43$, which we classify as strongly convective.

4.2. Baseline LODI Results

This evaluation is based on analysis of the 1-h averaged lateral dispersion parameter σ_y, crosswind-integrated concentrations (CWICs), and ground-level concentrations. For one experiment (day 1; September 14, 1978), there was no information provided on the MO length, friction velocity, and PBL depth, and therefore this day was not included in the evaluation. For another experiment (day 7; April 30, 1979), the crosswind concentration profiles were incomplete in that the concentrations on one side of the plume were not small or zero at the most distant lateral position. These profiles were not included in the σ_y and CWIC analyses, but were included in the surface concentration analysis.

4.2.1. Lateral Dispersion Parameter σ_y

We considered three ways of determining σ_y including: 1) a least-squares fit of a Gaussian profile to the observed crosswind profile, 2) a non-parameteric fit to the observed profile, and 3) the second-moment method. In the third approach, σ_y is found from

$$\sigma_y^2 = \frac{\int_{-\infty}^{\infty}(y-\overline{y})^2 C dy}{\int_{-\infty}^{\infty} C dy} \ , \tag{4.2}$$

where C is the mean concentration at point (x, y, z), x is the distance downwind of the source, y is the lateral (crosswind) distance from the mean plume centerline, height z is taken as zero in (4.2), and $\overline{y}$ is the y centroid position. There was little difference in the results from the three methods, and thus, we used the second-moment values since they are used most often in other studies including that of Gryning and Lyck (1984). In addition, the average ratio of the 1-h average σ_y determined by this method to the values given by Gryning and Lyck (1984) was 1.02 ± 0.02, thus ensuring consistency between our values and theirs.

Figure 1a compares the LODI predictions with the observed σ_y's, which were obtained over the range of 1.9 km $\leq x \leq$ 6.1 km. Overall, the observations are well-correlated with the predictions, which tend to overestimate the observations slightly on average, i.e., prediction $>$ observation. The overestimation is demonstrated by the dashed line, which corresponds to the geometric mean (MG) of the predicted-to-observed σ_y, and can be compared to the solid line representing equal values of $\sigma_{y\ LODI}$ and $\sigma_{y\ obs}$. The MG of $\sigma_{y\ LODI}/\sigma_{y\ obs}$ is 1.09 and the geometric standard deviation (GSD) of the ratio is 1.18. Despite the slight overprediction, these statistics are considered good and comparable to or better than those found for other models at other sites (e.g., Weil et al., 1997; Gryning et al., 1987).

In earlier work, Gryning et al. (1987) showed that Draxler's model agreed well with the Copenhagen data with little or no bias. They obtained their results using a constant T_D of 600 s along with the measured σ_v and mean wind speed U at the 120-m level on the tower. This U was assumed to be the average plume transport speed from which the transport time $t = x/U$ was determined. As a check on this, we compared the 120-m wind, U_{120}, with the CBL vertically-averaged wind from the MO profile, U_{MO}, and found $U_{120}/U_{MO} = 1.12$. Thus, the assumption appears to be reasonable.

A t based on a single or average wind speed is consistent with the homogeneous turbulence and wind field assumed in Draxler's model. The LODI implementation of Draxler's model differs in that the mean wind and turbulence (σ_v) fields are permitted to be vertically inhomogeneous, and the T_D is parameterized by Eq. (2.5), and thus is not constant from one experiment to the next. For the Copenhagen data, the LODI T_D ranged from about 300 s to 1000 s with an average of 611 s, which is close to the Gryning et al. value.

The slight overprediction by LODI in Fig. 1a could be due to the different treatments of the wind, turbulence, and T_D in LODI by comparison to those in Draxler (1976) and Gryning et al. (1987). As a test of this, we compared the Draxler model predictions, using the 120-m level values of σ_v and U, with the LODI predictions (Fig. 1b). The LODI parameterized T_D was used in both models so that the comparison addresses only the different wind and turbulence treatments in the two models. As can be seen, LODI predicts larger σ_y values with a geometric mean of $\sigma_{y\ LODI}/\sigma_{y\ Drax}$ of 1.27.

We believe that the larger LODI σ_y's are primarily due to the z-dependent wind profile in the model. In effect, LODI is double counting the wind shear effect since it is incorporated implicitly in Draxler's (1976) empirical choice of T_D and explicitly in the $U(z)$ adopted in ADAPT/LODI. The $U(z)$ results in a wind speed below the source that is less than U_{120}, and this leads to a greater plume/particle transport time to a receptor. The ratio $U_{120}/U_\ell = 1.34$, where U_ℓ is the average wind speed below the source as estimated from the MO profile. If we consider a constant σ_v, the σ_y ratio corresponding to two different transport times, t_1 and t_2, is $\sigma_{y2}/\sigma_{y1} = t_2/t_1$ for $t \ll T_D$ and $\sigma_{y2}/\sigma_{y1} = (t_2/t_1)^{1/2}$ for $t \gg T_D$. Thus, for $U_2 < U_1$ and $t_2 > t_1$, $\sigma_{y2} > \sigma_{y1}$ for either the short- or long-time regime.

The above analysis was carried further by computing the σ_{y2}/σ_{y1} ratio using the Draxler form for f_D (Eq. 2.4b), the LODI T_D for each experiment/day, and assuming that σ_v was the same in the two calculations (σ_{y2} and σ_{y1}). With these assumptions and $U_1/U_2 = 1.34$, we found the GM of σ_{y2}/σ_{y1} to be 1.25, which is close to the value found in Fig. 1b. This supports the contention that the LODI σ_y's are larger than those from Draxler principally because of the height-dependent wind in LODI.

We would expect that with a uniform wind and the same T_D as in Draxler, the σ_y values in the two models should be the same. Figure 2a shows that the LODI σ_y computed in this manner with $T_D = 800$ s is approximately equal to the Draxler σ_y, i.e., the two values differ by only 6% on average. For the same T_D but a z-dependent wind profile in LODI, the LODI σ_y's exceed the Draxler values by 22% on average; this is generally consistent with the result in Fig. 1b.

In addition to wind speed shear effects, the wind direction shear included in LODI would

broaden the plume (e.g., see Venkatram, 1988). Further analysis of the modeled σ_y behavior is presented in Section 4.3.

4.2.2. Crosswind-Integrated Concentration at the Surface

The mean crosswind-integrated concentration (CWIC), C^y, is defined by

$$C^y(x,z) = \int_{-\infty}^{\infty} C(x,y,z)dy \ . \tag{4.3}$$

For a vertically-uniform wind, the surface CWIC is primarily a measure of the vertical dispersion since the CWIC is independent of the lateral concentration distribution and σ_y. Thus, the ability of a model to match the observed CWIC is principally a test of its vertical dispersion prediction.

In the following, we first discuss the behavior of the expected CWIC field as found from laboratory experiments and numerical simulations. Then, we present and analyze the LODI CWIC results and compare them with 1) the Copenhagen data, and 2) numerical simulations of dispersion obtained with another Lagrangian particle dispersion model (LPDM) (Weil, 2003; Weil et al., 2004) in which the particle velocities are driven by large-eddy simulations (LESs).

Our understanding of dispersion is most complete for the strong convection case due largely to the laboratory experiments of Willis and Deardorff (1976, 1978, 1981). For a near-surface source of height $z_s = 0.07z_i$, Willis and Deardorff (1976) found that the mean plume centerline as defined by the locus of maximum CWIC ascended after a short distance ($x \simeq 0.5Uz_i/w_*$). In contrast, the centerline from an elevated source ($z_s/z_i = 0.24$) descended until it reached the surface. The ascent of the near-surface plume resulted from the "sweep out" of material near the surface by updrafts before the material carried aloft earlier (by stronger updrafts) recirculated down. The descent of the elevated plumes was due to the large time scale of the convective motion and the greater area occupied by downdrafts than updrafts (Lamb, 1982).

Willis and Deardorff also presented the surface CWIC in the dimensionless form C^yUz_i/Q, where Q is the source strength and $Q/(Uz_i)$ is the vertically well-mixed CWIC far downstream, i.e., at large distances, $C^yUz_i/Q = 1$. The CWICs were given as a function of the dimensionless distance X:

$$X = \frac{w_* x}{U z_i} \ , \tag{4.4}$$

which is the ratio of the plume travel time x/U to the eddy turnover time z_i/w_*; as noted earlier, the T_L is of the order of z_i/w_*.

Figure 3 presents the dimensionless CWIC from the laboratory experiments (points) for releases at $z_s/z_i = 0.07$ and 0.24. In both cases, the CWIC exhibits 1) a local surface maximum as expected for an elevated source (Pasquill and Smith, 1983), 2) an approach to the well-mixed CWIC ($C^yUz_i/Q = 1$) at $X \simeq 3$, and 3) an undershoot of the well-mixed value over the range $1 \leq X \leq 2$. The undershoot is due to the "sweep out" phenomena discussed above (see also Lamb, 1982; Weil, 1988a). A comparison of Figs. 3a and 3b shows the significant reduction in the maximum CWIC (by about a factor of 3) and the

greater distance to the maximum with an increase in the source height from $z_s/z_i = 0.07$ to 0.24 (e.g., see also Briggs, 1983; Lamb, 1982; Weil, 1988a).

In addition, Fig. 3 presents CWIC predictions from the Weil et al. (2004) LPDM, which is driven by LES velocity fields. In this combined LPDM–LES approach, one decomposes the Lagrangian velocity of a passive "particle" into resolved and subgrid-scale (SGS) components consistent with the LES, where the SGS component used in the particle tracking is a random velocity based on the LES SGS turbulent kinetic energy (TKE). Figure 3a shows the LPDM results for three stability indices with those for strong convection ($-z_i/L = 106$) being most applicable to the laboratory data and indeed matching the data well. The results for moderate and weak convection ($-z_i/L = 16$, 5.5) show that the maximum CWIC and the CWICs downstream of the maximum increase with a decrease in $-z_i/L$. This is caused by the reduced vertical dispersion, which is attributed to the greater wind shear and the higher TKE dissipation rates and lead to smaller turbulence time scales, especially near the surface.

Figure 4 shows LODI predictions of the surface CWIC for each day of the Copenhagen experiments. The observations generally were obtained near or beyond the location of the LODI maximum CWIC, which typically ranged from 1 km to 2 km downwind. Overall, the predictions are in reasonable agreement with the observations. The agreement is demonstrated further by the scatter plot in Fig. 5, where there is a good correlation between the predictions and observations. In addition, all of the predictions are within a factor of 2 of the observations. The LODI values are essentially unbiased (Fig. 5) as shown by the MG of the ratio C^y_{LODI}/C^y_{obs}: the $MG = 0.97$, and the GSD of the ratio is 1.32. We consider these statistics to be good based on comparisons of other models at other sites (e.g., Weil et al., 1997).

Despite the above agreement, there is a tendency in some cases for LODI to underestimate the CWIC near the maximum value and the magnitude of the slope $\partial C^y/\partial x$ over the range 2 km $\leq x \leq 6$ km; e.g., see Fig. 4a, b, f, g, and h. The ratio of the LODI maximum CWIC to the highest observed value ranges from about 0.74 to 1.

To help understand the cause of some of these near-source underpredictions, we compared LODI to the LPDM predictions. The LPDM is based on a more fundamental approach to particle modeling in that: 1) it uses the Lagrangian three-dimensional velocity of a particle and includes the velocity time correlation, 2) the LES velocity fields driving the model are based on the filtered Navier-Stokes equations for the resolved velocity and parameterizations of the less-energetic SGS velocities, and 3) the LES velocity statistics show good agreement with laboratory and field observations (Moeng and Wyngaard, 1989). Thus, there is an expectation that the LPDM, which matches the laboratory data well in strong convection (Fig. 5), also will be a good predictor in weaker convection. However, the LPDM results only are available for three values of $-z_i/L$—106, 16, and 5.5. Hence, we use the LPDM results from the most representative case or cases for each of the Copenhagen experiments.

Figure 6 presents the dimensionless CWIC at the surface as a function of X for LODI, the LPDM, and the observations for each day of the experiments. With one exception, the

dimensionless source heights fall in the range $0.055 \leq z_s/z_i \leq 0.14$. For day 2 (Fig. 6a) which is the most convective case, results from two LPDM predictions ($-z_i/L = 16,\ 106$) are given and are found to bracket the observations, which were obtained for an intermediate $z_i/|L|$ ($= 43$). For all other days, the LPDM results are presented for the most representative $-z_i/L$ value. Note that the difference in the magnitude of the dimensionless CWIC on days with the same $-z_i/L$ value is due to the different dimensionless source heights, e.g., see Figs. 6b, d, e, and h.

Three general observations can be made from the comparisons in Fig. 6: 1) the LPDM maximum CWIC typically exceeds the LODI maximum by a factor up to 1.5, 2) the LPDM CWIC and the dimensionless gradient $\partial C^{y*}/\partial X$ downstream of the maximum generally agree better with the observations than do the LODI values, where the dimensionless CWIC $C^{y*} = C^y U z_i/Q$, and 3) LODI has a more gradual rise and fall in the CWIC upstream and downstream, respectively, of the CWIC maximum. That is, LODI has a smaller gradient $|\partial C^{y*}/\partial X|$ than does the LPDM.

The difference between the LPDM and the observations for day 2 (Fig. 6a) are well within the statistical uncertainty in C^y for strong convection as computed using the LPDM-LES approach (Weil, 2003). For example, at the distance X_{max} ($\simeq 0.15$) of the maximum mean CWIC, the computed scatter in C^y (Max C^y/Min C^y) is about a factor of 5, whereas further downstream ($X \simeq 0.7$) it increases to ~ 10; see Weil (2003). The uncertainty calculations were based on 30 individual realizations of the CWIC field. The uncertainty was computed only for the strong convection case, but it is expected to be of a similar magnitude or somewhat smaller for the moderate and weak convection cases in Figs. 6b to 6h. (Assuming a lognormal probability distribution for C^y, the factor of 5 and 10 scatterbands above would lead to a GSD in C^y of about 1.3 and 1.5, respectively.)

The underestimation of the maximum mean CWIC by LODI is believed due to two causes: 1) the use of the eddy-diffusion approach instead of a more general vertical dispersion parameterization that includes a finite T_L (e.g., a Lagrangian stochastic model for w), and 2) the absence of vertical velocity skewness, S_w. The $S_w = \overline{w^3}/\sigma_w^3$, where $\overline{w^3}$ is the third moment of the vertical velocity fluctuations. The effect of S_w on vertical dispersion and mixing is stronger the greater the T_L as shown by Weil (1990) and Wyngaard and Weil (1991).

For homogeneous turbulence and zero skewness, the surface CWIC maximum, C^y_{max}, is independent of the form of the $\sigma_z(x)$ expression. This can be shown with the Gaussian plume model, which gives the surface C^y as

$$C^y = \frac{2Q}{\sqrt{2\pi} U \sigma_z} \exp\left(-\frac{z_s^2}{2\sigma_z^2}\right) \ . \tag{4.5}$$

The C^y_{max} is found by setting $\partial C^y/\partial x = 0$, where $\partial C^y/\partial x$ is given by

$$\frac{\partial C^y}{\partial x} = C^y \left(\frac{z_s^2}{\sigma_z^2} - 1\right) \frac{1}{\sigma_z} \frac{\partial \sigma_z}{\partial x} \ . \tag{4.6}$$

This equation shows that the $\partial C^y/\partial x = 0$ and hence the maximum CWIC occurs when

$\sigma_z = z_s$, regardless of the form of $\sigma_z(x)$; the C^y_{max} is found to be

$$C^y_{max} = \frac{2Q}{(2\pi e)^{1/2} U z_s} \ . \tag{4.7}$$

Although C^y_{max} is independent of the form of $\sigma_z(x)$, the distance to the maximum, x_{max}, depends on $\sigma_z(x)$. This can be shown using the limiting forms of vertical dispersion from Taylor's (1921) theory for homogeneous turbulence

$$\sigma_z = \sigma_w t \qquad t \ll T_L \tag{4.8a}$$

$$\sigma_z = (2\sigma_w^2 T_L t)^{1/2} \qquad t \gg T_L \ , \tag{4.8b}$$

where the form for large t (Eq. 4.8b) is consistent with K-theory with the $K_z = \sigma_w^2 T_L$. By setting $t = x/U$ and $\sigma_z = z_s$, we find that the maximum CWIC occurs at a distance $x_{max1} = z_s/(\sigma_w/U)$ for $\sigma_z \propto t$ and at distance $x_{max2} = z_s^2/(2\sigma_w^2 T_L/U)$ for $\sigma_z \propto t^{1/2}$. [Note that $x_{max1} = x_{max1}$ if $T_L = \sigma_w/(2z_s)$.]

In the CBL, vertical velocity skewness has values ranging from 0.4 to 1 (Wyngaard, 1988), and it produces significantly higher maximum CWIC's at the surface than does a Gaussian probability density function (PDF) or one with a zero skewness. Weil (1988a) showed this using an analytical "PDF" dispersion model based on a parameterized w PDF and a large T_L. The model results for a skewed w PDF agreed well with convection tank experiments (Willis and Deardorff, 1976, 1978) and numerical simulations (Lamb, 1982). Weil found that the ratio of the maximum CWIC with skewness ($S_w = 0.6$) to that without it was about 1.75, thus demonstrating the importance of the w skewness. We believe that the absence of S_w in LODI together with use of the eddy-diffusion approach (i.e., for a small rather than a large T_L) may explain the range of the CWIC ratios, $C^y_{max\ LPDM}/C^y_{max\ LODI}$, of 1 to 1.5 found in Fig. 6. Thus, we conclude that: 1) a vertical dispersion model incorporating a finite T_L, and 2) vertical velocity skewness both are necessary to match the maximum CWICs given by the LPDM.

The above diagnosis of the LODI and LPDM results uses dispersion models based on homogeneous turbulence. Now we analyze the eddy-diffusion approach in LODI and consider the effect of the vertical inhomogeneity in K_z (Eq. 2.3) on the maximum CWICs. In Lagrangian random-walk dispersion models, the mean vertical drift velocity w_{dr} of particles is up-the-gradient of K_z (Durbin, 1983; Rodean, 1996):

$$w_{dr} = \frac{\partial K_z}{\partial z} \ , \tag{4.9}$$

which is included in the LODI particle displacement equation (2.2). For LODI, the w_{dr} is found by differentiating Eq. (2.3) with respect to z and is

$$w_{dr} = \frac{k u_*}{\phi_h} \exp\left(\frac{-c_k z}{z_i}\right) \left[1 - \frac{z}{\phi_h}\frac{\partial \phi_h}{\partial z} - \frac{c_k z}{z_i}\right] \ . \tag{4.10}$$

In the CBL, we find the term $(1/\phi_h)\partial\phi_h/\partial z = 8/(L\phi_h^4)$ using Eq. (2.3), and it is negative since $L < 0$. Therefore, w_{dr} initially increases with height due to the second term in the

brackets of Eq. (4.10), attains a maximum value, and then decreases due to the third term in the brackets. The $w_{dr} = 0$ at some height z_{w0}, where the bracketed quantity is zero and at large heights where the exponential term in (4.10) dominates.

Figure 7a presents the ratio of the maximum CWICs from LODI and the LPDM, C^y_{LODI}/C^y_{LPDM}, as a function of w_{dr}/u_*, where w_{dr} is computed at the source height. With perhaps the exception of one or two points, there is a good correlation between the CWIC ratio and w_{dr}/u_*—the ratio decreases with an increase in w_{dr}. As discussed earlier, the plume centerline (locus of maximum CWIC) from an elevated source in the CBL descends due to the greater areal coverage of downdrafts than updrafts. However, with an eddy-diffusion model, the greater the drift velocity (Eq. 4.10), the greater would be the tendency of the model to keep particles aloft in opposition to the natural mean plume or particle descent. Thus, the larger w_{dr}'s would lower the maximum CWIC relative to the LPDM, consisent with the behavior found in Fig. 7a.

Figure 7b presents the maximum CWIC ratio as a function of the dimensionless source height z_s/z_i and shows an increasing C^y_{LODI}/C^y_{LPDM} with increasing z_s/z_i. This is consistent with the tendency of w_{dr} to decrease for heights in the range $z_{wm} < z < z_{w0}$, where z_{wm} is the height at which the maximum w_{dr} is attained. Note that the largest CWIC ratio occurs for the largest dimensionless source height, $z_s/z_i = 0.29$, which also coincides with the smallest w_{dr}/u_* (Fig. 7a).

The purpose of Figs. 6 and 7 and the associated discussion was to help understand the cause of the deviations of the LODI predictions from the LPDM and observations and to consider physical effects which could improve the predictions. Overall, these deviations are not large—less than a factor of 2—and the agreement of LODI with the observations is considered good.

The comparisons generally dealt with relatively low source heights (z_s/z_i), and it would be useful to have a more complete assessment of LODI performance in the CBL. This should include a) source heights throughout the entire CBL, b) buoyant releases, and c) stronger instability ($-z_i/L > 43$). In addition, it is recommended that two alternative approaches be considered for modeling short-range dispersion from an elevated source. The first is a Lagrangian plume (or puff) model in which a meandering plume with a specified spatial concentration distribution (e.g., a Gaussian) is advected using a Lagrangian stochastic model of the plume centroid velocity. The second is a Lagrangian stochastic model of the particle velocity with subsequent integration to obtain the particle displacement. The first approach would be computationally faster, and in both approaches the stochastic model would account for the finite T_L effects and any plume/particle buoyancy; e.g., a "hybrid" stochastic approach was given by Weil (1994) but others are possible. The intent of such an approach is to handle near-source dispersion and buoyancy effects in a practical way in keeping with the overall LODI philosophy/approach. Modeling of the concentration field by one of the above approaches would be conducted for $t \leq \alpha T_L$, where $\alpha = 1$ to 3, and by the existing LODI for larger travel times or distances. Merging of the hybrid approach with the existing LODI model would be conducted to achieve a smooth transition between the two models.

4.2.3. Surface Concentrations

The maximum surface concentration along the y axis—the arc-maximum concentration C_{mx}—as a function of downstream distance is shown in Fig. 8 for each day of the Copenhagen experiments. The observations exhibit mean trends and data scatter about the LODI predictions that are similar to the CWIC results (Fig. 4). In addition, the gradient $|\partial C_{mx}/\partial X|$ for the observations downwind of the maximum prediction is typically larger than that given by LODI (see Figs. 8a, b and Figs. 8f to 8i). Despite this, the overall agreement between LODI and the observations is considered good. Further evidence of the agreement is demonstrated by the scatter plot in Fig. 9, which shows a good correlation between the predictions and observations. LODI is biased slightly toward underprediction and has an MG of the predicted-to-observed C_{mx} of 0.88, with a GSD of the ratio of 1.49. These statistics are judged to be good by comparison to other models at other locations (Weil et al., 1997).

In addition, we made a point-by-point comparison of the LODI predictions with the observations, i.e., predictions and observations paired in both space and time. Figure 10a shows this for all 265 non-zero concentrations both on and off the plume centerline. The comparison is similar to Fig. 9 in that LODI is biased toward underprediction with the MG of C_{LODI}/C_{obs} given by 0.78, but it differs from Fig. 9 in that the data scatter is substantially greater; here, the GSD of C_{LODI}/C_{obs} is 5.1. One of the major reasons for the large scatter is the difference between the observed and predicted wind directions as discussed below. Other reasons are the: 1) stochastic variability in the concentration, and 2) uncertainties in the model inputs (e.g., see Weil et al., 1992).

Figure 10b presents a quantile-quantile (Q-Q) plot of the observed and LODI-predicted concentrations. The results are obtained by ordering the C_{LODI} and C_{obs} values from lowest to highest and plotting the concentrations corresponding to the same rank in each distribution. This is not a rigorous test of model performance, but it is helpful for determining if the overall distributions or cumulative distribution functions (CDFs), regardless of the space and time pairing, are close or the same for the model and observations; this is especially useful for air quality applications (e.g., Cimorelli et al., 1996; Perry et al., 2005). As can be seen, the results fall close to the 1:1 line, indicating good agreement between the two CDFs.

The uncertainty or difference between the predicted and observed wind direction is a common problem in modeling point source plume dispersion (e.g., see Weil et al., 1992). Small differences of only a few degrees ($\sim 2^\circ$ to 10°) between the two directions can lead to large differences between the predicted and observed concentrations. Figure 11 shows that the observed wind direction Θ_{obs} is correlated well with the LODI-predicted direction Θ_{LODI} over the range of measurements; the directions are obtained from the location of the arc-maximum concentration. The mean direction difference $\overline{\Delta\Theta}$ is only 1.2°, where

$$\Delta\Theta = \Theta_{LODI} - \Theta_{obs} \ . \tag{4.11}$$

However, the root-mean-square (rms) deviation is 8.6°, and the mean absolute difference $|\overline{\Delta\Theta}| = 7.4^\circ$.

A parameter that measures the importance of the direction uncertainty or difference is $|\Delta\Theta|/(\sigma_v/U_{120})$, where the denominator is proportional to the lateral plume spread σ_y. This can be seen from Eq. (2.4a) by replacing t by x/U_{120}. We then have $\sigma_y = \sigma_v x/U_{120} \cdot f_D$ and $\sigma_y/x = (\sigma_v/U_{120})f_D$, where σ_y/x measures the angle subtended by σ_y at distance x. For small values of $|\Delta\Theta|/(\sigma_v/U_{120})$ (i.e., $\ll 1$), the direction uncertainty should have little effect on the predictions, but for parameter values ~ 1 or > 1, the direction difference can lead to lateral displacements of the same order or larger than σ_y, and hence to large concentration differences, $C_{LODI} - C_{obs}$. With the Copenhagen data, $|\Delta\Theta|/(\sigma_v/U_{120})$ ranged from 0 to 1.6 with an average value of 0.74 and an rms value of 0.51. Thus, the direction differences can lead to large concentration differences.

Based on the above results and discussion, we reran the comparisons between the LODI and observed concentrations using the observed direction Θ_{obs} to orient the plume. The purpose was to determine how much improvement would occur in the model performance. Figure 12a is a replot of the point-by-point comparisons for this case of a "shifted direction" and again only nonzero concentrations are included. The GM of C_{LODI}/C_{obs} is 0.86 and slightly closer to the ideal value (1) than found in Fig. 10a. Moreover, the scatter appears to be subtantially reduced by comparison to Fig. 10a although the GSD of the ratio C_{LODI}/C_{obs} only falls to 4 from 5.1 in Fig. 10a. However, most of the large scatter occurs for the lower concentration region, e.g., for $C_{obs} < 300$ ng/m^3. The ranked distributions in the Q-Q plot (Fig. 12b) are much the same as in Fig. 10b albeit slightly closer to the 1:1 line.

The predictions and observations also were analyzed in terms of the mean fractional error, $\overline{f_e}$, where the fractional error is given by

$$f_e = \frac{2(C_p - C_o)}{C_p + C_o} \ , \tag{4.12}$$

and C_p and C_o are the predicted and observed concentrations, respectively. There are two advantages of this statistic: 1) it is symmetric in terms of the degree of overprediction ($C_p/C_o > 1$) and underprediction ($C_p/C_o < 1$), and 2) it is well-behaved in the limits of zero values of C_p and/or C_o. The first point means that for a ratio $r = C_p/C_o$ say of 2 which corresponds to $f_e = 2/3$, whereas for $r = 0.5$, $f_e = -2/3$. For reference, the ratio $C_p/C_o = 1.25$, 1.5, 2, 3, and 5 correspond to $f_e = 0.22$, 0.4, 0.67, 1, and 1.33, respectively.

The 309 point-by-point comparisons between predicted and observed concentrations resulted in a $\overline{f_e} = -0.01$, a rms fluctuation $\sigma_{f_e} = 1.21$, and a percentage of predictions within a factor of 2 of the observations $Fac2 = 38\%$. The above $\overline{f_e}$ corresponds to a mean ratio of C_p/C_o of 0.99. Figure 13a presents $\overline{f_e}$ and σ_{f_e} as a function of the experiment day for all concentrations. The scatter of the daily mean f_e about the zero line (dashed) is within the rms fluctuation in f_e.

To remove the effect of the wind direction uncertainty, we repeated the comparisons by setting $\Theta_{LODI} = \Theta_{obs}$. The comparisons resulted in an overall $\overline{f_e} = 0.16$, a $\sigma_{f_e} = 1.08$, and a $Fac2 = 51\%$. Figure 13b shows the day-to-day variation in $\overline{f_e}$ and σ_{f_e} for the "shifted direction." The reduction in the σ_{f_e} and the increase in $Fac2$ by comparison to results for the "unshifted direction" (Fig. 13a) is consistent with the removal of the wind direction

uncertainty. However, the increase in $\overline{f_e}$ and its greater deviation from zero is unexpected. We believe that the main reason for the latter result is due to C_p, C_o comparisons at the plume tails. For the unshifted direction, there are a number of cases at the tails in which $C_p, C_o = 0, 0$ and $f_e = 0$. However, with the shifted plume direction, a number of these cases are replaced by $C_p > 0$, $C_o = 0$, which leads to $f_e = 2$ (see Eq. 4.12). The net result is that with the shifted direction, more $f_e = 2$ values are added to the overall statistics, which leads to the positive bias (0.16) in $\overline{f_e}$.

Figure 14 presents the $\overline{f_e}$ and σ_{f_e} results for comparisons restricted to nonzero concentrations. For the shifted direction (Fig. 14b), there is a marked improvement in the overall (all days) performance statistics—$\overline{f_e} = -0.06$, $\sigma_{f_e} = 0.88$, and $Fac2 = 58\%$—by comparison to the results for the unshifted direction (Fig. 14a), where $\overline{f_e} = -0.19$, $\sigma_{f_e} = 1.06$, and $Fac2 = 41\%$. In addition, the results in Fig. 14b are better than those found for the "All concentration" cases in Fig. 13.

4.3. σ_y Sensitivity to Wind Profile and T_D

The sensitivity of σ_y to the mean wind profile shape and T_D was investigated using the 1-hr averaged σ_y predictions. The modified σ_y values are labeled by $\sigma_{y\ CTD}$ denoting a contant T_D (CTD) to distinguish them from the original LODI σ_y values. For the $\sigma_{y\ CTD}$, the wind profile was either the height-dependent $U(z)$ profile given by ADAPT or a uniform wind with speed $U = U_{120}$ from the Copenhagen tower. Three T_D values—200 s, 800 s, and 3200 s—were chosen to cover a broad time-scale range, which includes the 1000 s recommended by Draxler (1976) and the 600 s found by Gryning et al. (1987). The motivation for including the uniform wind was that Draxler's (1976) model is based on Taylor's (1921) theory, which applies to homogeneous turbulence and a homogeneous wind field; in the model, $t = x/U$ where U is the average wind speed.

Figure 15 compares the observed and predicted σ_y for a uniform wind (U_{120}) and the three T_D values. As can be seen, a $T_D = 800$ s provides the best agreement with observations for the three T_D's shown, and this T_D is intermediate to the value (1000 s) recommended by Draxler (1976) and the 600 s found by Gryning and Lyck (1984).

Figure 16 compares the observed σ_y with the $\sigma_{y\ CTD}$ values for the height-dependent wind speed ($U(z)$) and direction from ADAPT and the three T_D values used above. Based on these results, we estimate that a best-fit T_D would be in the range of 200 s to 400 s. A simple explanation for the smaller best-fit T_D (than in Fig. 15) is the same as given earlier—the transport time to a receptor is greater due to the wind speed shear and reduced wind below the source. Thus, the function $f_D = 1/[1 + 0.9(t/T_D)^{1/2}]$ in Eq. (2.4) must be decreased to compensate for the greater effective transport time t; hence, a smaller T_D is required.

A statistical summary of the results from Figs. 15 and 16 is presented in Fig. 17, which shows the MG of the ratio $\sigma_{y\ CTD}/\sigma_{y\ obs}$ (points) along with the GSD (vertical lines). The dotted line is a simple empirical fit (by eye) to the MGs. For the results with the $U(z)$ (Fig. 17b), a run was added for a $T_D = 400$ s, and the result ($MG = 1.05$) is close to the ideal ratio of 1.

5. Summary and Conclusions

The NARAC model was evaluated using observed concentration fields downwind of an elevated point source in the CBL with emphasis on the dispersion component LODI. The observations were obtained from the Copenhagen experiment (Gryning and Lyck, 1984), which consisted of passive tracer (SF_6) releases from a 115-m tall source and surface concentration measurements along three downwind arcs. The CBL stability was characterized mainly as weakly-to-moderately convective based on the stability index $-z_i/L$. The NARAC/LODI evaluation included comparisons between predicted and observed values of the 1-h averaged crosswind dispersion parameter σ_y, the crosswind-integrated concentrations (CWICs), and the ground-level concentrations.

The LODI σ_y predictions were in good overall agreement with the Copenhagen data with an MG of the predicted-to-observed σ_y of 1.09 and a relatively small scatter. Further analysis of the LODI σ_y was made by comparing it with Draxler's (1976) model, the basis of the LODI σ_y parameterization. Draxler's formulation assumes uniform wind and turbulence fields in accord with Taylor's (1921) theory, whereas LODI adopts a z-dependent wind profile. The LODI wind profile assumption results in longer transport times and hence larger σ_y values than Draxler (by about a factor of 1.3) for the same dispersion time scale T_D. Agreement between the two models and between each model and observations can be achieved by using an appropriate T_D in each, with a smaller value required in LODI. The LODI σ_y agreement with observations suggests that its T_D parameterization is satisfactory for the CBL.

The LODI surface CWIC predictions were essentially unbiased showing an MG of the predicted-to-observed values of 0.97 with a GSD of the ratio of 1.32. These statistics were considered quite good, but there was some tendency for LODI to underestimate the observations near the maximum CWIC. A diagnosis of LODI was made using a more detailed approach—a Lagrangian particle dispersion model (LPDM) driven by velocity fields from large-eddy simulations. Comparisons of the two models showed that LODI typically underestimated the maximum CWIC by a factor ranging from 0.67 to 1 and exhibited a smaller gradient $|\partial C^y/\partial x|$ than the LPDM, i.e., a more gradual rise and fall of the CWIC upstream and downstream of the maximum. The LODI behavior was expected because of the use of an eddy-diffusion approach, which neglects the effects of a large Lagrangian time scale T_L and the CBL's vertical velocity skewness (see Section 4.2.2). Despite the modest underpredictions of the CWIC maxima, the overall agreement of LODI with the CWIC observations was considered good.

Analysis of the maximum surface concentration C_{mx} showed that the LODI trends versus distance and the data were similar to those of the surface CWIC. For the C_{mx}, LODI exhibited relatively good agreement with the data, but was biased slightly toward underprediction with an MG of the predicted-to-observed values of 0.88 and a GSD in the ratio of 1.49. A point-by-point comparison of LODI with all of the nonzero observations showed some underprediction (MG of C_{LODI}/C_{obs} of 0.78); however, the data scatter was far greater than for the C_{mx} with a GSD in the predicted-to-observed concentration ratio of 5.1. This result was attributed mainly to the deviation between the predicted and observed wind directions (see Section 4.2.3) but also to the stochastic variability in the

concentrations and the meteorological input uncertainties. Comparisons using the observed wind direction to orient the plume showed better agreement between LODI and the observations—an MG of C_{LODI}/C_{obs} of 0.86, a GSD in the ratio of 4, and 58% of the predictions within a factor of 2 of the observations.

6. References

Briggs, G.A., 1975: Plume rise predictions. *Lectures on Air Pollution and Environmental Impact Analyses*, D.A. Haugen, Ed., Amer. Meteor. Soc., Boston, 59–111.

Briggs, G.A., 1985: Analytical parameterizations of diffusion: the convective boundary layer. *J. Climate Appl. Meteor.*, **24**, 1167–1186.

Briggs, G.A., 1993: Plume dispersion in the convective boundary layer. Part II: Analyses of CONDORS field experiment data. *J. Appl. Meteor.*, **32**, 1388–1425.

Caughey, S.J., 1982: Observed characteristics of the atmospheric boundary layer. *Atmospheric Turbulence and Air Pollution Modelling*, F.T.M. Nieuwstadt and H. van Dop, Eds., Reidel, Dordrecht, 107–158.

Chang, J.C., P. Franzese, K. Chayantrakom, and S.R. Hanna, 2003: Evaluations of CALPUFF, HPAC, and VLSTRACK with two mesoscale field datasets. *J. Appl. Meteor.*, **42**, 453–466.

Cimorelli, A.J., S.G. Perry, R.F. Lee, R.J. Paine, A. Venkatram, J.C. Weil, and R.B. Wilson, 1996: Current progress in the AERMIC model development program, Paper 96-TP24B.04 in *Proceedings of the 89th Annual Meeting & Exhibition of the Air and Waste Management Association*, Pittsburgh, PA.

Csanady, G.T., 1973: *Turbulent Diffusion in the Environment*, Reidel, 248 pp.

Deardorff, J.W., 1972: Numerical investigation of neutral and unstable planetary boundary layers. *J. Atmos. Sci.*, **29**, 91–115.

Draxler, R.R., 1976: Determination of atmospheric diffusion parameters. *Atmos. Environ.*, **10**, 99–105.

Durbin, P.A., 1983: Stochastic differential equations and turbulent dispersion. NASA Ref. Pub. 1103, 69 pp.

Ermak, D.L., and J.S. Nasstrom, 2000: A Lagrangian stochastic diffusion method for inhomogeneous turbulence. *Atmos. Environ.*, **34**, 1059–1068.

Gryning, S.-E., and E. Lyck, 1984: Atmospheric dispersion from elevated sources in an urban area: comparison between tracer experiments and model calculations. *J. Climate Appl. Meteor.*, **23**, 651–660.

Gryning, S.E., A.A.M. Holtslag, J.S. Irwin, and B. Sivertsen, 1987: Applied dispersion modelling based on meteorological scaling parametera. *Atmos. Environ.*, **21**, 79–89.

Hicks, B.B., 1985: Behavior of turbulent statistics in the convective boundary layer. *J. Climate Appl. Meteor.*, **24**, 607–614.

Holtslag, A.A.M., and C.-H. Moeng, 1991: Eddy diffusivity and countergradient transport in the convective atmospheric boundary layer. *J. Atmos. Sci.*, **48**, 1690–1698.

Lamb, R.G., 1978: A numerical simulation of dispersion from an elevated point source in the convective planetary boundary layer. *Atmos. Environ.*, **12**, 1297–1304.

Lamb, R.G., 1982: Diffusion in the convective boundary layer. *Atmospheric Turbulence and Air Pollution Modeling*, F.T.M. Nieuwstadt and H. van Dop, Eds., Reidel, 159–229.

Lange, R., 1989: Transferability of a three-dimensional air quality model between two different sites in complex terrain. *J. Appl. Meteor.*, **28**, 665–679.

Moeng, C.-H., and J.C. Wyngaard, 1989: Evaluation of turbulent transport and dissipation closures in second-order modeling. *J. Atmos. Sci.*, **46**, 2311–2330.

Nasstrom, J.S., G. Sugiyama, J.M. Leone, Jr., and D.L. Ermak, 2000: A real-time atmospheric dispersion modeling system. *Preprints 11th Joint Conference on the Applications of Air Pollution Meteorology with the AWMA*, Amer. Meteor. Soc., Boston, 84–89.

Nieuwstadt, F.T.M., 1980a: An analytic solution of the time-dependent one-dimensional diffusion equation in the atmospheric boundary layer. *Atmos. Environ.*, **14**, 1361–1364.

Nieuwstadt, F.T.M., and H. van Durren, 1978: Dispersion experiments with SF_6 from the 213 m high meteorological mast at Cabauw in the Netherlands. Preprints *Fourth Symposium on Turbulence, Diffusion, and Air Pollution*, Amer. Meteor. Soc., Boston.

Pasquill, F.A., and F.B. Smith, 1983: *Atmospheric Diffusion* (third ed.). Wiley, New York, 437 pp.

Perry, S.G., A.J. Cimorelli, R.J. Paine, R.W. Brode, J.C. Weil, A. Venkatram, R.B. Wilson, R.F. Lee, and W.D. Peters, 2005: AERMOD: A dispersion model for industrial source applications. Part II: Model performance against seventeeen field-study databases. To appear in: *J. Appl. Meteor.*

Rodean, H.C., 1996. *Stochastic Lagrangian Models of Turbulent Diffusion*, *Meteorological Monographs*, **26**, No. 48, Amer. Meteor. Soc., Boston, 84 pp.

Smith, F.B., 1957: The diffusion of smoke from a continuous elevated point source into a turbulent atmosphere. *J. Fluid Mech.*, **2**, 49.

Sugiyama, G., and S.T. Chan, 1998: A new meteorological data assimilation model for real-time emergency response. *Preprints 10th Joint Conference on Air Pollution Meteorology with the AWMA*, Amer. Meteor. Soc., Boston, 285–289.

Sugiyama, G., J.S. Nasstrom, H.-N. S. Chin, K.T. Foster, D.J. Larson, M.J. Leach, J.M. Leone, Jr., D. Maddix, J.E. Tull, and H. Walker, 2002: Advancement of a real-time atmospheric dispersion modeling system. *Preprints 12th Joint Conference on Air Pollution Meteorology with the AWMA*, Amer. Meteor. Soc., Boston, 1–2.

Taylor, G.I., 1921: Diffusion by continuous movements. *Proc. London Math. Soc. Ser. 2*, **20**, 196–212.

Venkatram, A., 1988: Dispersion in the stable boundary layer. *Lectures on Air Pollution Modeling*, A. Venkatram and J.C. Wyngaard, Eds., Amer. Meteor. Soc., Boston, 228–265.

Weil, J.C., 1988a: Dispersion in the convective boundary layer. *Lectures on Air Pollution Modeling*, A. Venkatram and J.C. Wyngaard, Eds., Amer. Meteor. Soc., Boston, 167–227.

Weil, J.C., 1988b: Plume rise. *Lectures on Air Pollution Modeling*, A. Venkatram and J.C. Wyngaard, Eds., Amer. Meteor. Soc., Boston, 119–166.

Weil, J.C., 1990: A diagnosis of the asymmetry in top-down and bottom-up diffusion using a Lagrangian stochastic model. *J. Atmos. Sci.*, **47**, 501–515.

Weil, J.C., 1994: A hybrid Lagrangian dispersion model for elevated sources in the convective boundary layer. *Atmos. Environ.*, **28**, 3433–3448.

Weil, J.C., 2003: Collaborative Research: Lagrangian Modeling of Dispersion in the Planetary Boundary Layer. Final report to U.S. Army Research Office from University of Colorado, Boulder, Contract No. DAAG55-97 1 0259, 17 pp.

Weil, J.C., R.I. Sykes, and A. Venkatram, 1992: Evaluating air-quality models: Review and outlook. *J. Appl. Meteor.*, **31**, 1121–1145.

Weil, J.C., L.A. Corio, and R.P. Brower, 1997: A PDF dispersion model for buoyant plumes in the convective boundary layer. *J. Appl. Meteor.*, **36**, 982–1003.

Weil, J.C., P.P. Sullivan, and C.-H. Moeng, 2004: The use of large-eddy simulations in Lagrangian particle dispersion models. *J. Atmos. Sci.*, **61**, 2877–2887.

Willis, G.E., and J.W. Deardorff, 1976: A laboratory model of diffusion into the convective planetary boundary layer. *Quart. J. Roy. Meteor. Soc.*, **102**, 427–445.

Willis, G.E., and J.W. Deardorff, 1978: A laboratory study of dispersion from an elevated source within a modeled convective planetary boundary layer. *Atmos. Environ.*, **12**, 1305–1312.

Willis, G.E., and J.W. Deardorff, 1981: A laboratory study of dispersion from a source in the middle of the convectively mixed layer. *Atmos. Environ.*, **15**, 109–117.

Wyngaard, J.C., 1988: Structure of the PBL. *Lectures on Air Pollution Modeling*, A. Venkatram and J.C. Wyngaard, Eds., Amer. Meteor. Soc., Boston, 9–61.

Wyngaard, J.C., and J.C. Weil, 1991: Transport asymmetry in skewed turbulence. *Phys. Fluids A*, **3**, 155–162.

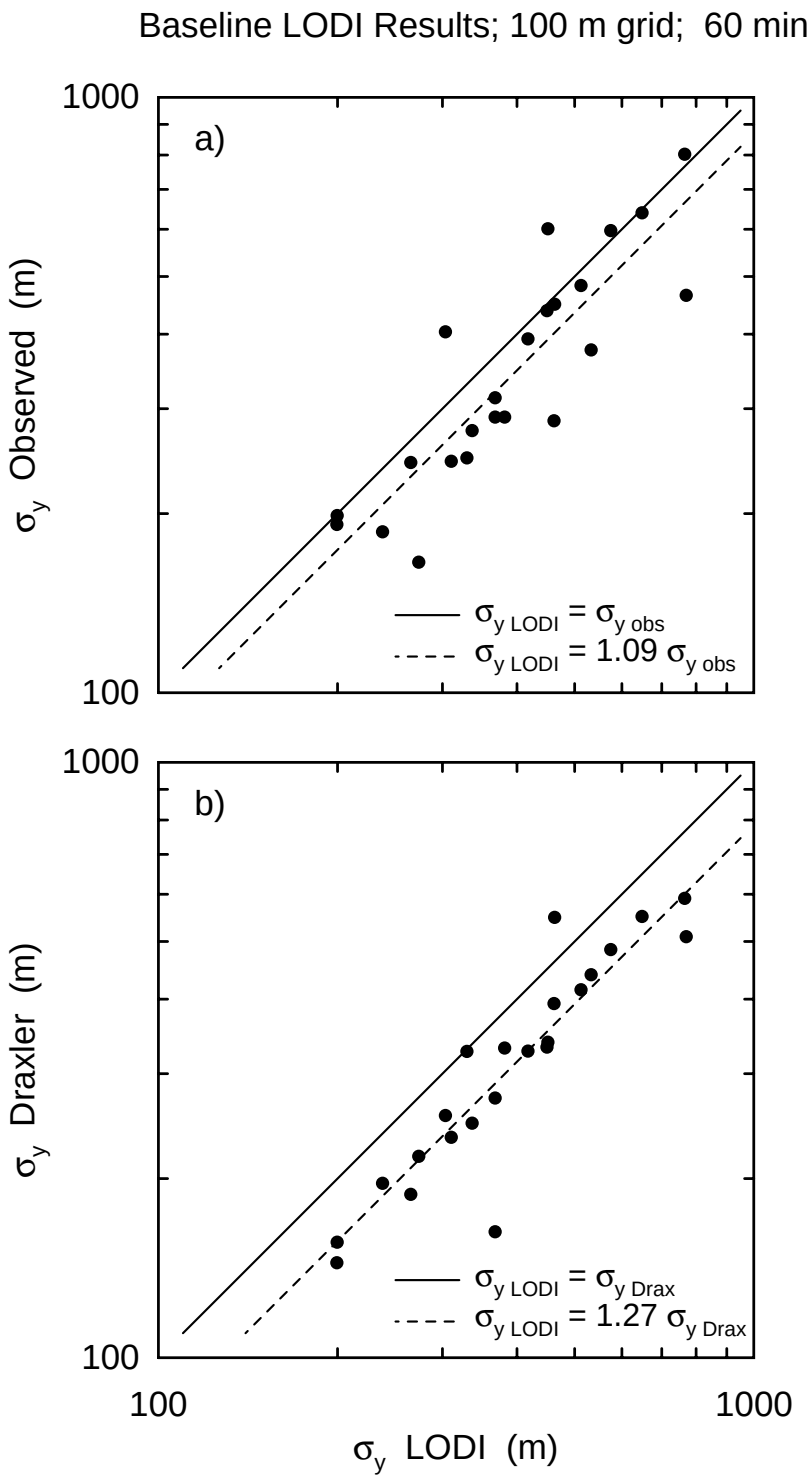

Figure 1: Comparison between a) observed 1-h lateral dispersion parameter σ_y and LODI predictions, and b) Draxler (1976) and LODI σ_y predictions using the LODI parameterized T_D.

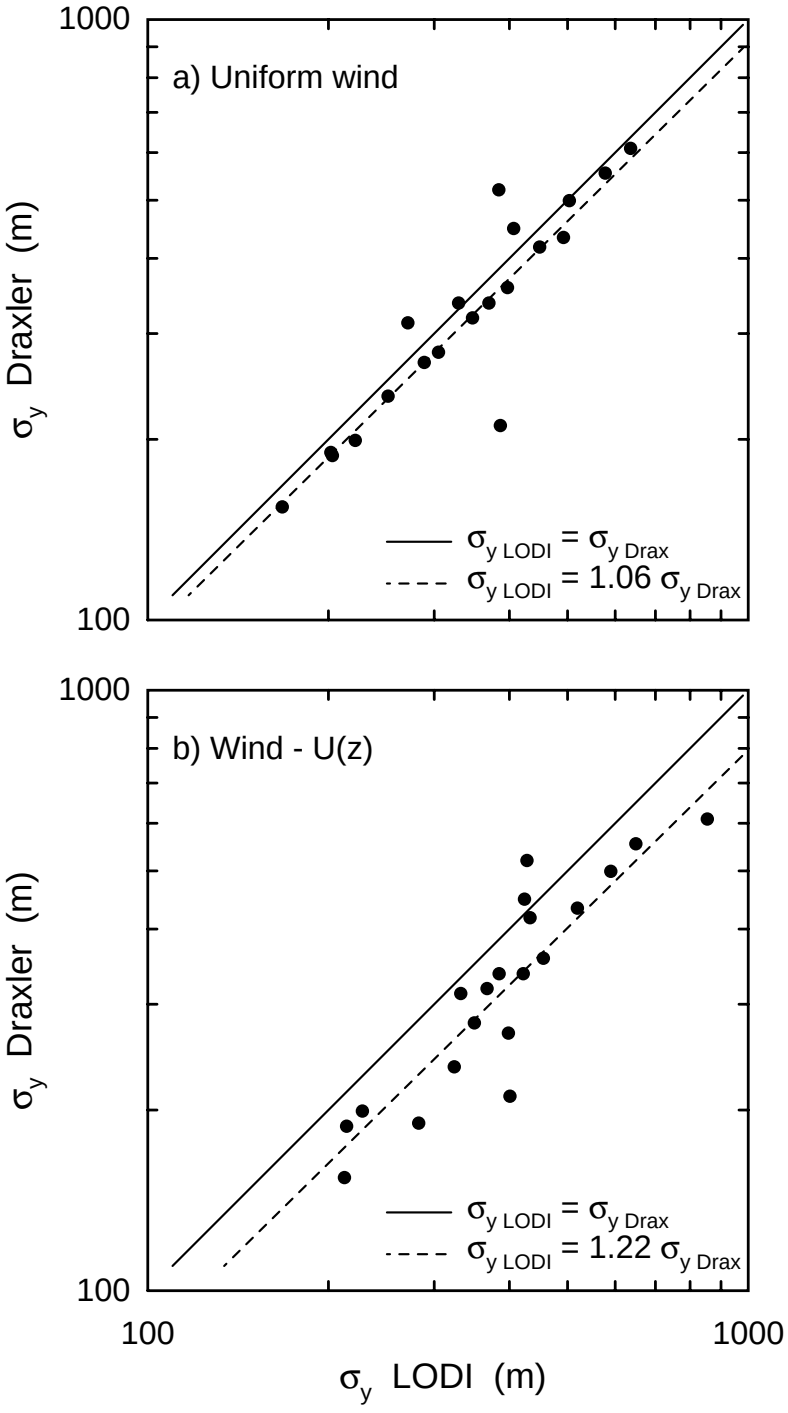

Figure 2: Comparison between Draxler (1976) and LODI predictions of the 1-h σ_y for: a) a vertically uniform wind profile, and b) the height-dependent wind profile in LODI; in both models $T_D = 800$ s.

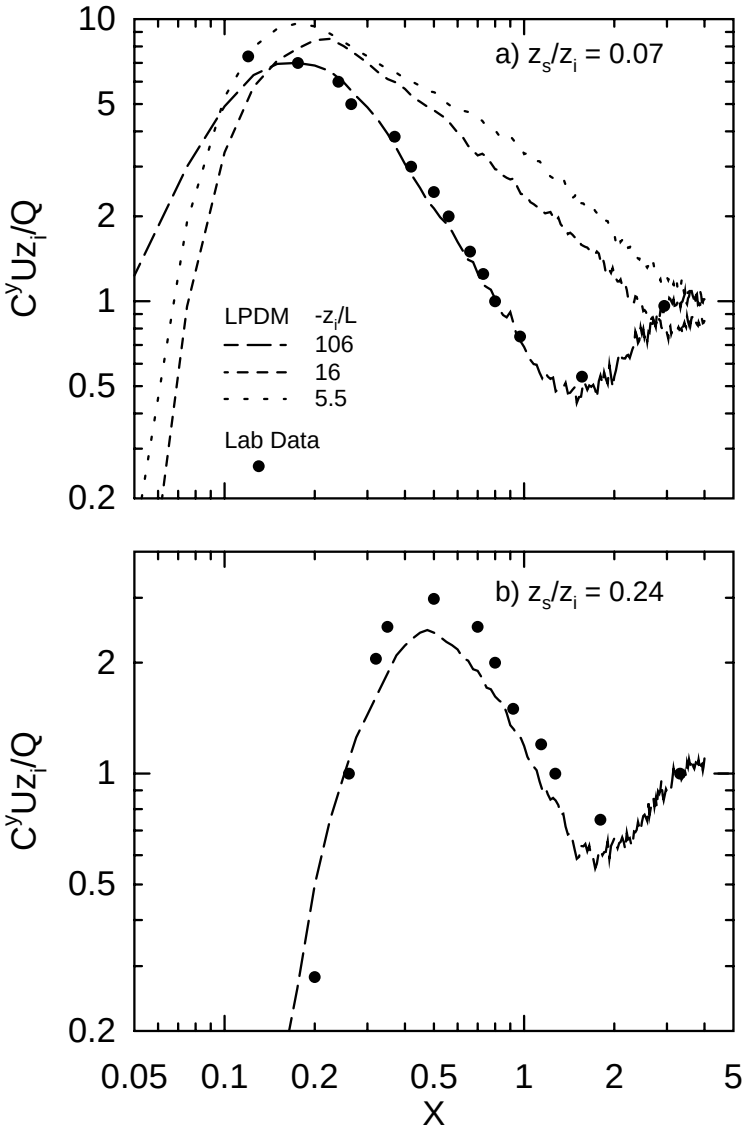

Figure 3: Dimensionless crosswind-integrated concentration at the surface as a function of dimensionless distance X for passive releases at two heights in the convective boundary layer. Laboratory data are from Willis and Deardorff (1976, 1978) and Lagrangian particle dispersion model (LPDM) predictions are from Weil (2003) and Weil et al. (2004).

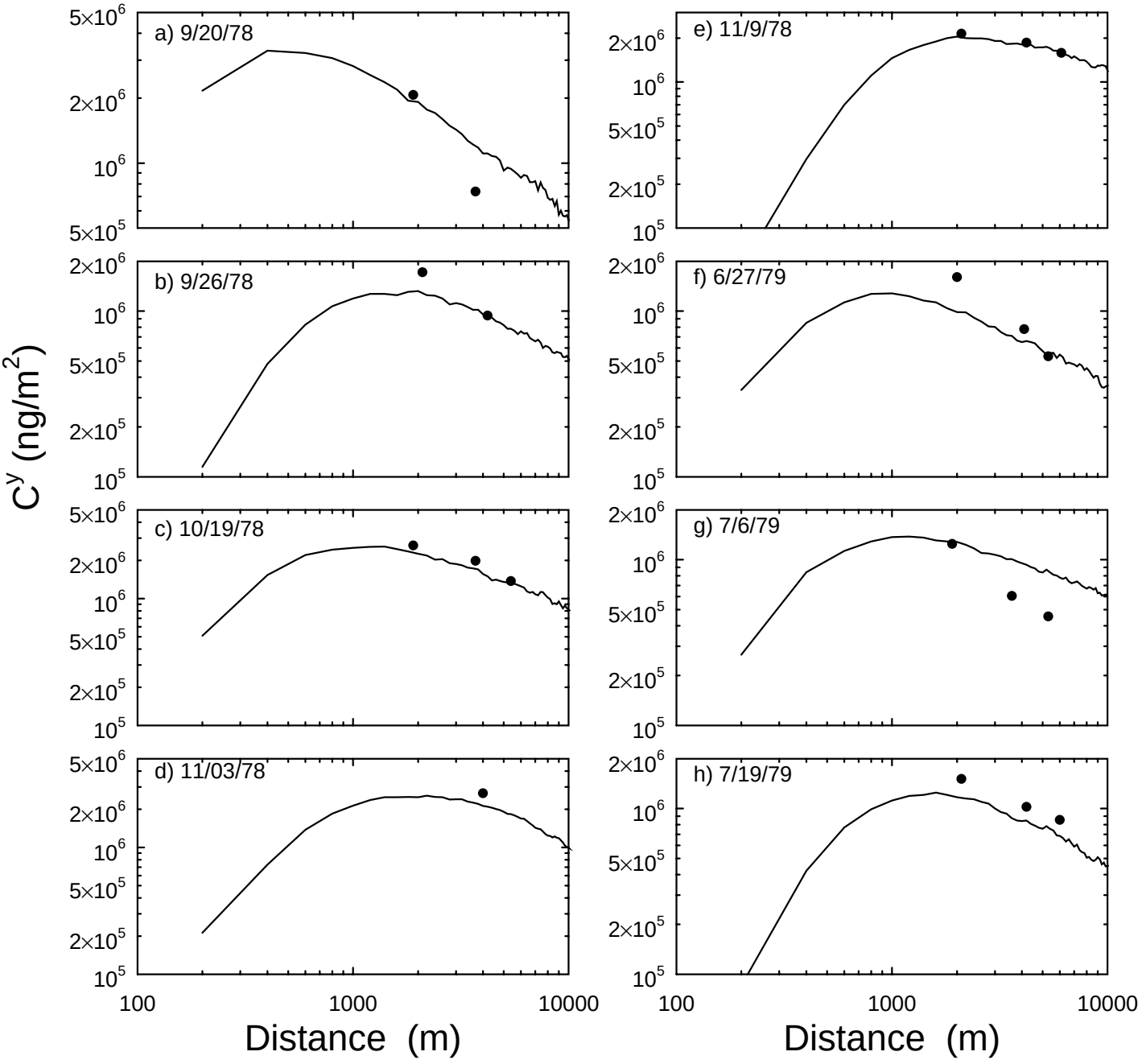

Figure 4: Comparison between LODI predictions (lines) and observed 1-h averages (points) of crosswind-integrated concentration at the surface versus downwind distance for the Copenhagen experiments.

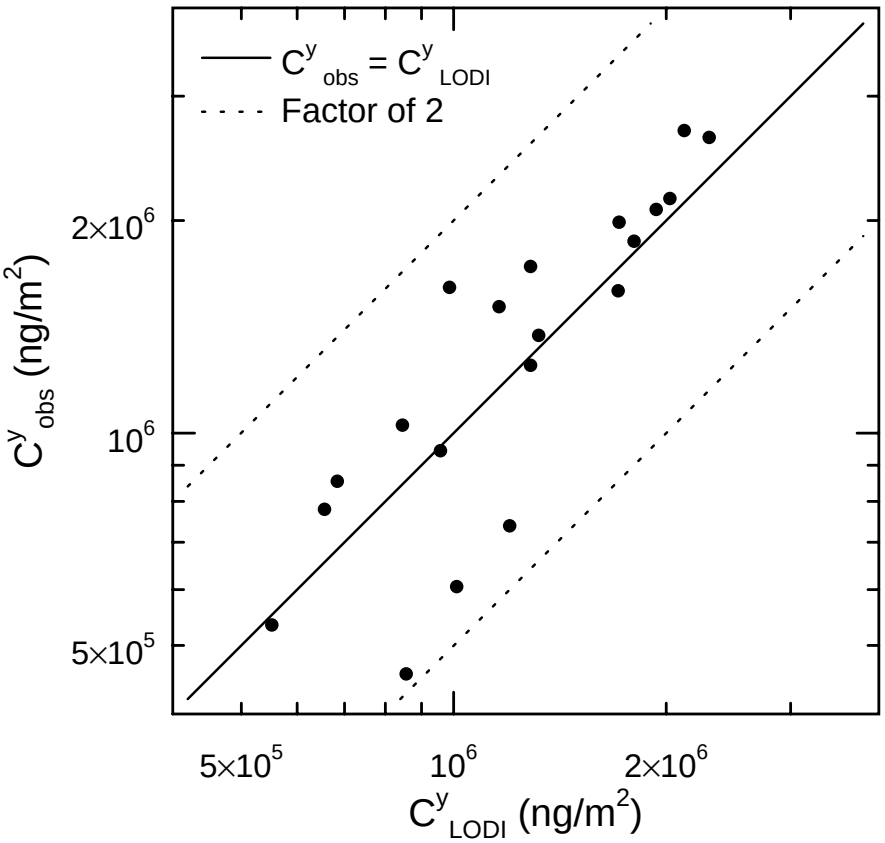

Figure 5: Comparison between observed 1-h averages and LODI predictions of the crosswind-integrated concentration at the surface for all Copenhagen experiments except day 7; dotted lines correspond to factor of 2 over- and under-prediction.

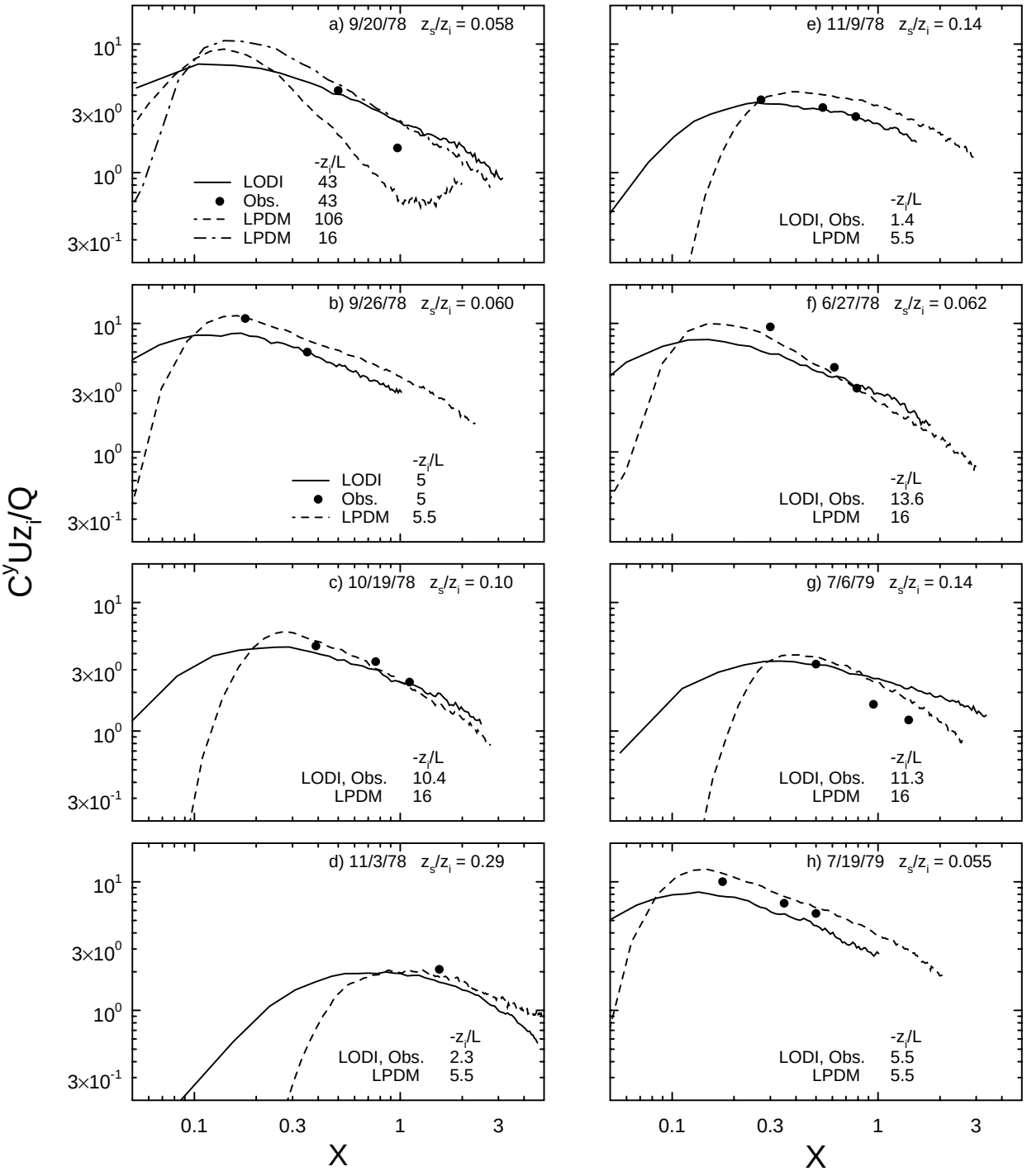

Figure 6: Dimensionless crosswind-integrated concentration at the surface as a function of the dimensionless downwind distance for all Copenhagen experiments except day 7. The Lagrangian particle dispersion model (LPDM) results are from Weil (2003) and Weil et al. (2004).

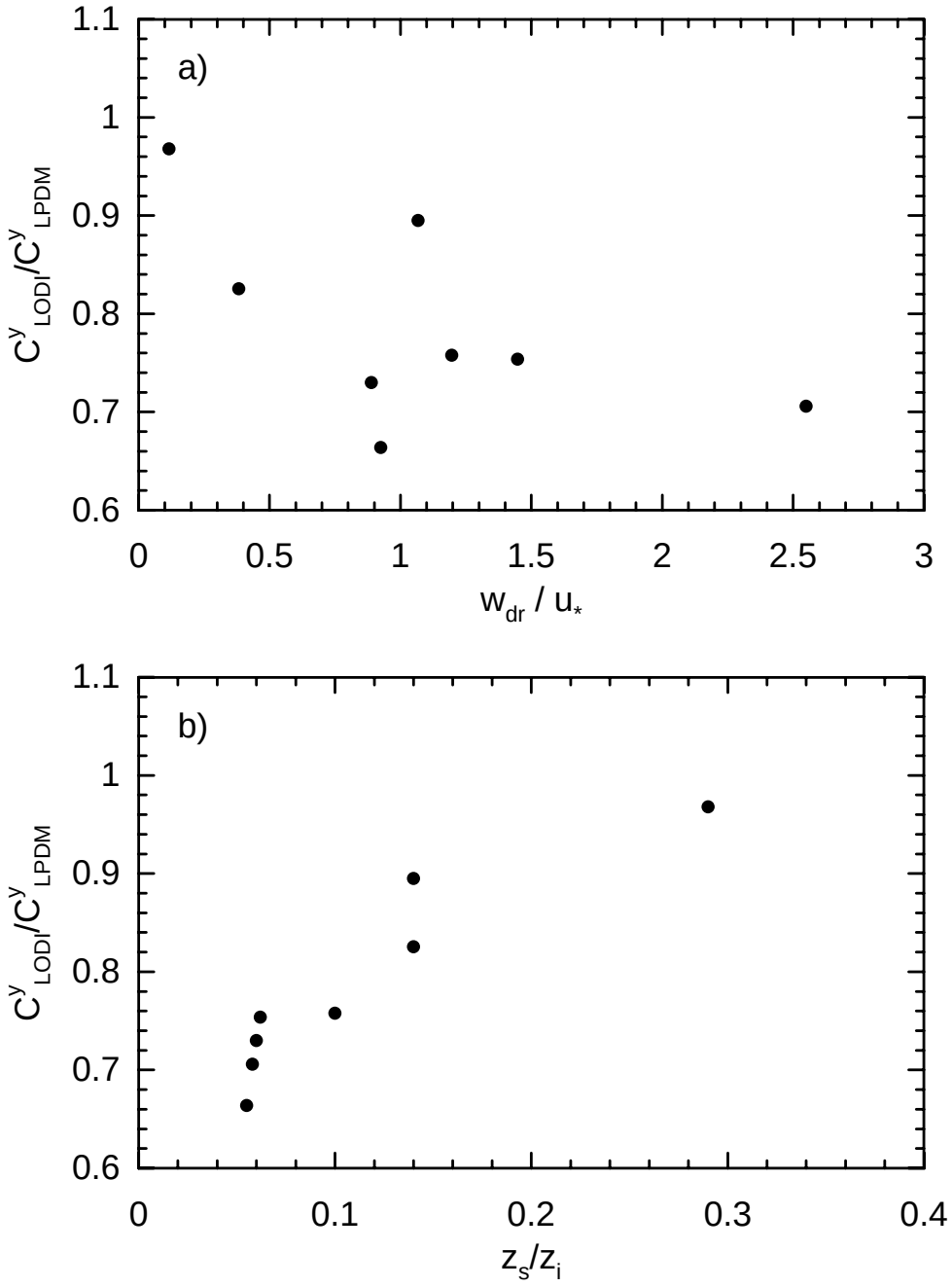

Figure 7: Ratio of the maximum crosswind-integrated concentration predicted by LODI and the LPDM (Fig. 6) as a function of a) the LODI drift velocity (at z_s) nondimensionalized by the friction velocity, and b) the dimensionless source height.

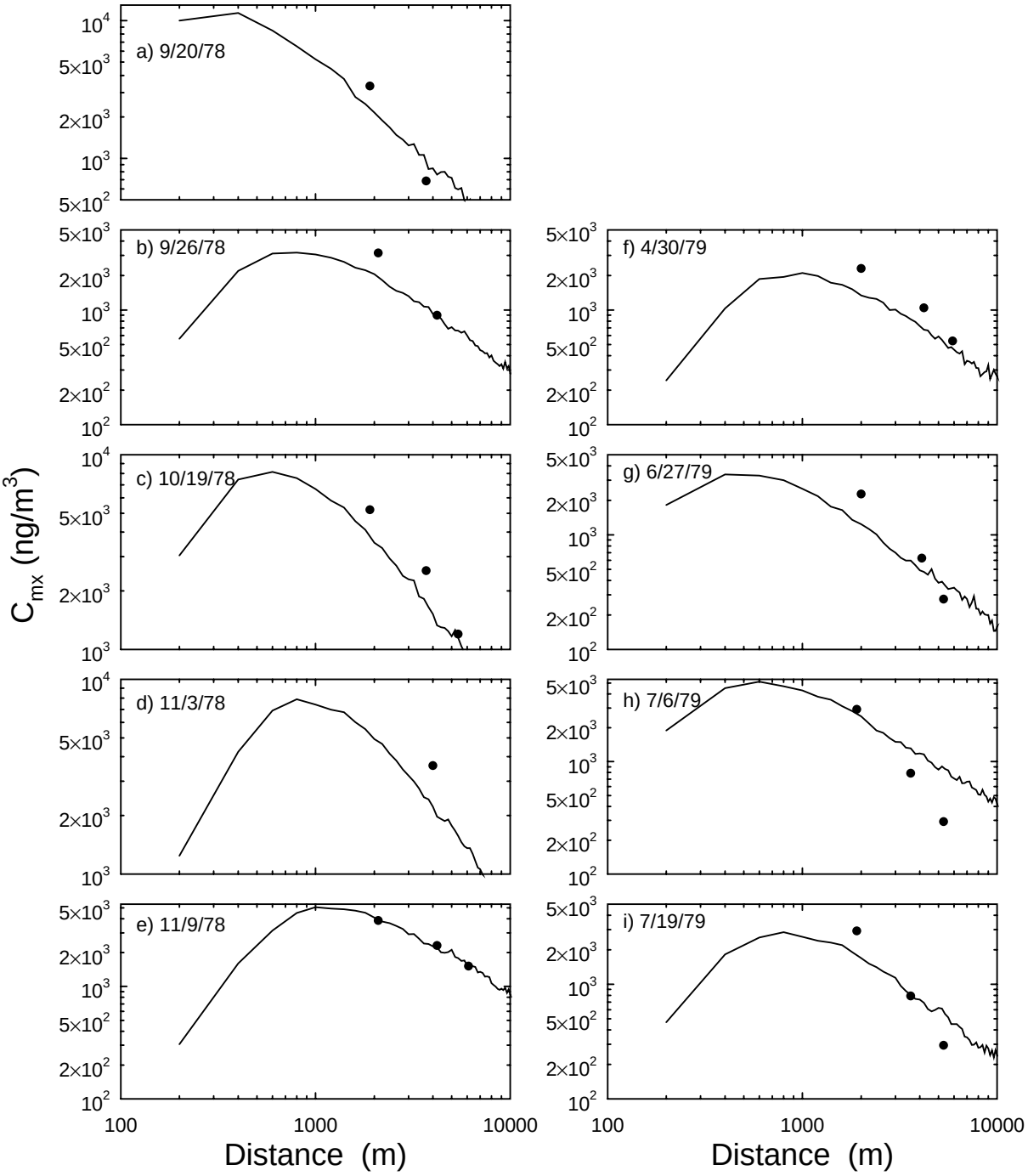

Figure 8: Comparison between LODI predictions (lines) and observed 1-h averages of the surface arc-maximum concentration as a function of downwind distance.

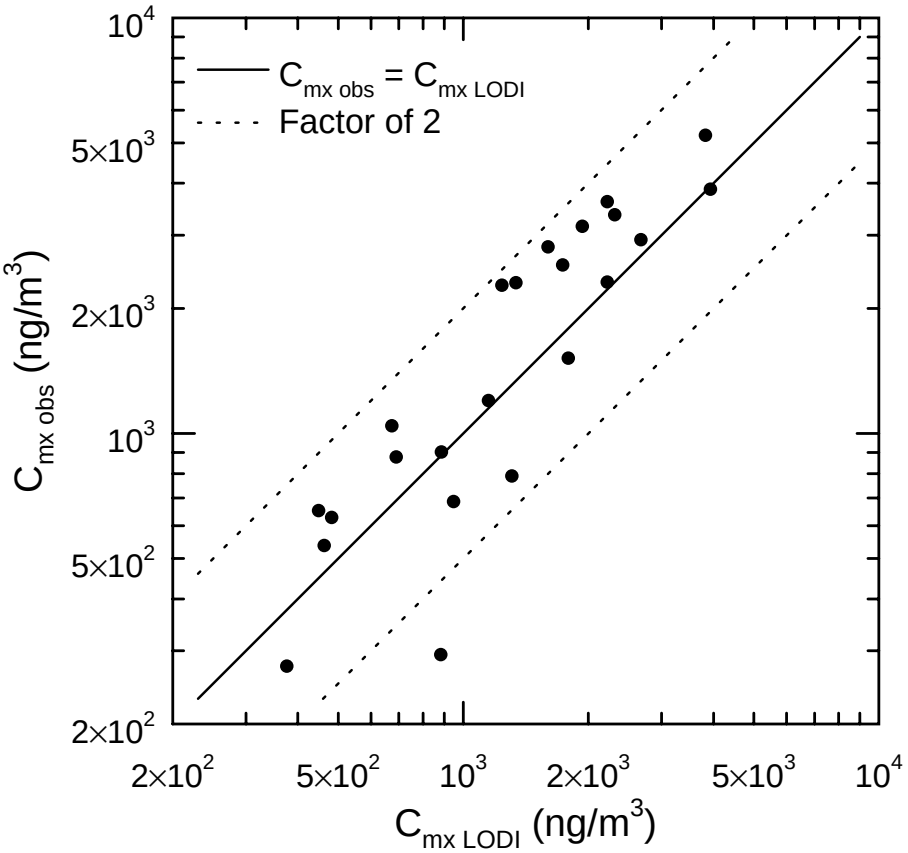

Figure 9: Observed 1-h averaged values versus LODI predictions of arc-maximum concentrations at the surface for all days of Copenhagen experiments; dotted lines correspond to factor of 2 over- and under-prediction.

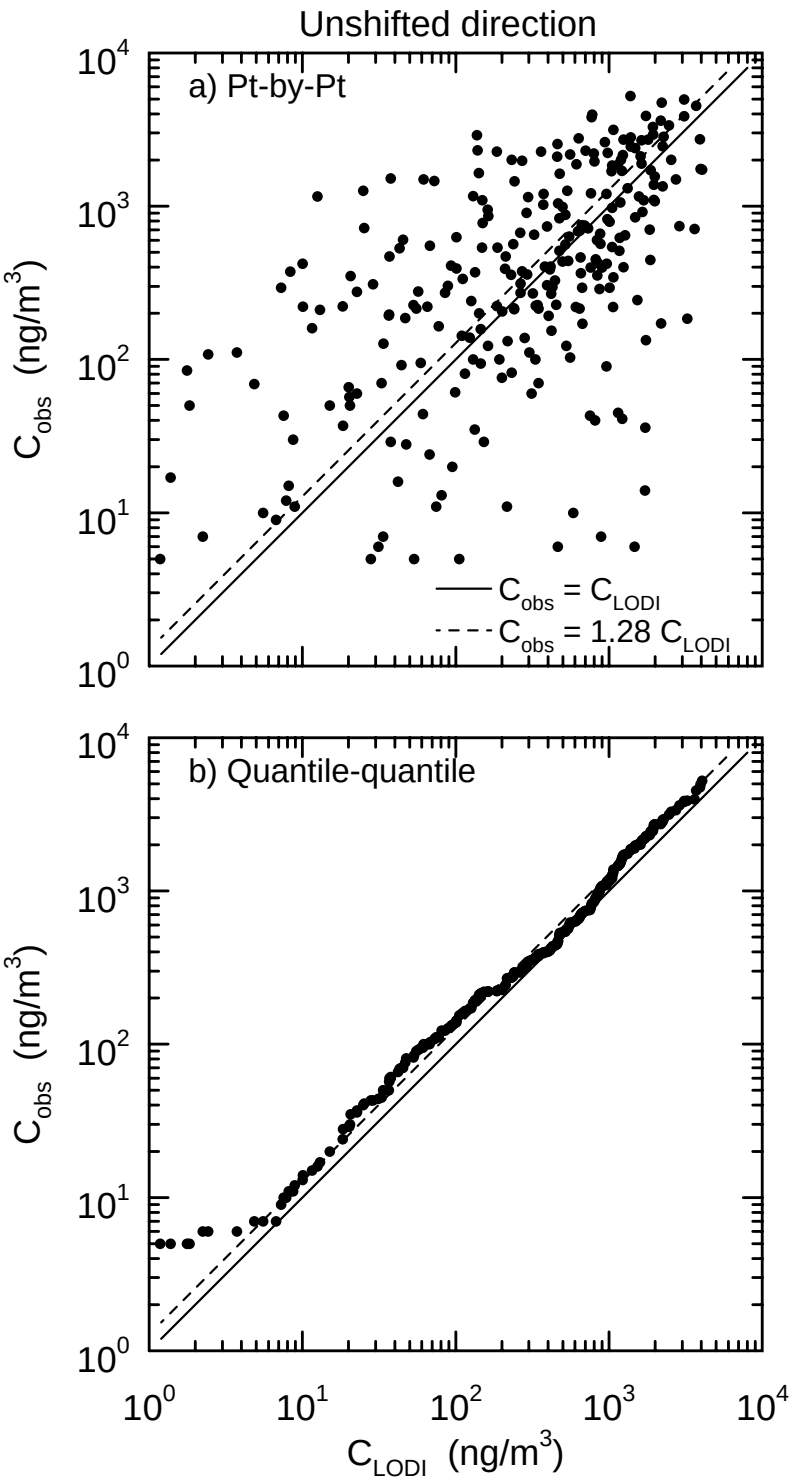

Figure 10: Observed 1-h values versus LODI predictions of ground-level concentrations in the Copenhagen experiment: a) point-by-point comparison, and b) quantile-quantile comparison; only nonzero concentrations included. Dashed line corresonds to geometric mean (0.78) of C_{LODI}/C_{obs}, where the geometric standard deviation of the ratio is 5.1. LODI modeled wind direction used in predictions.

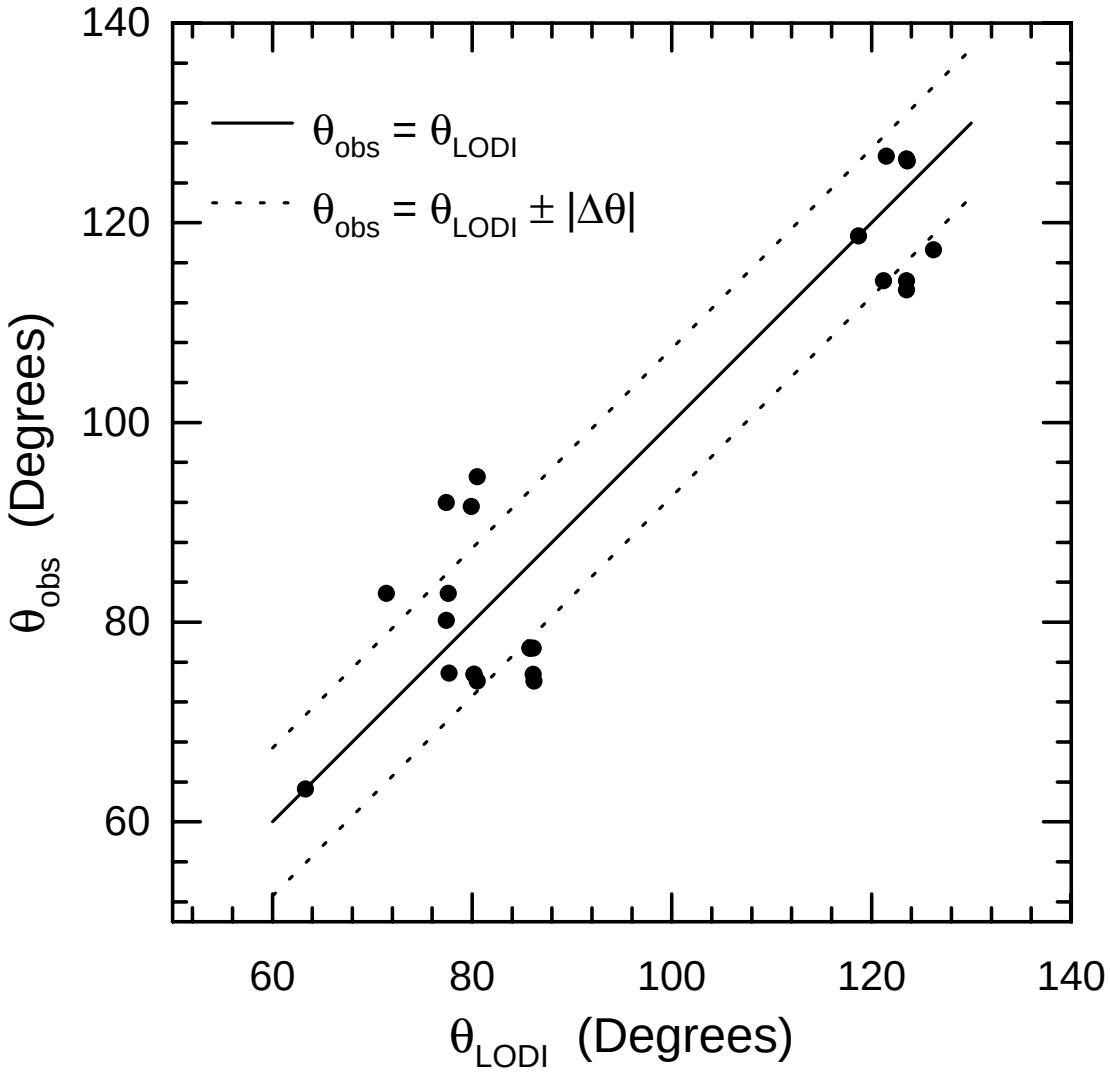

Figure 11: Observed versus predicted plume direction for each arc and day in the Copenhagen experiment; dashed line corresponds to the mean absolute difference in direction, $|\Delta\Theta| = |\Theta_{LODI} - \Theta_{obs}| = 7.4°$.

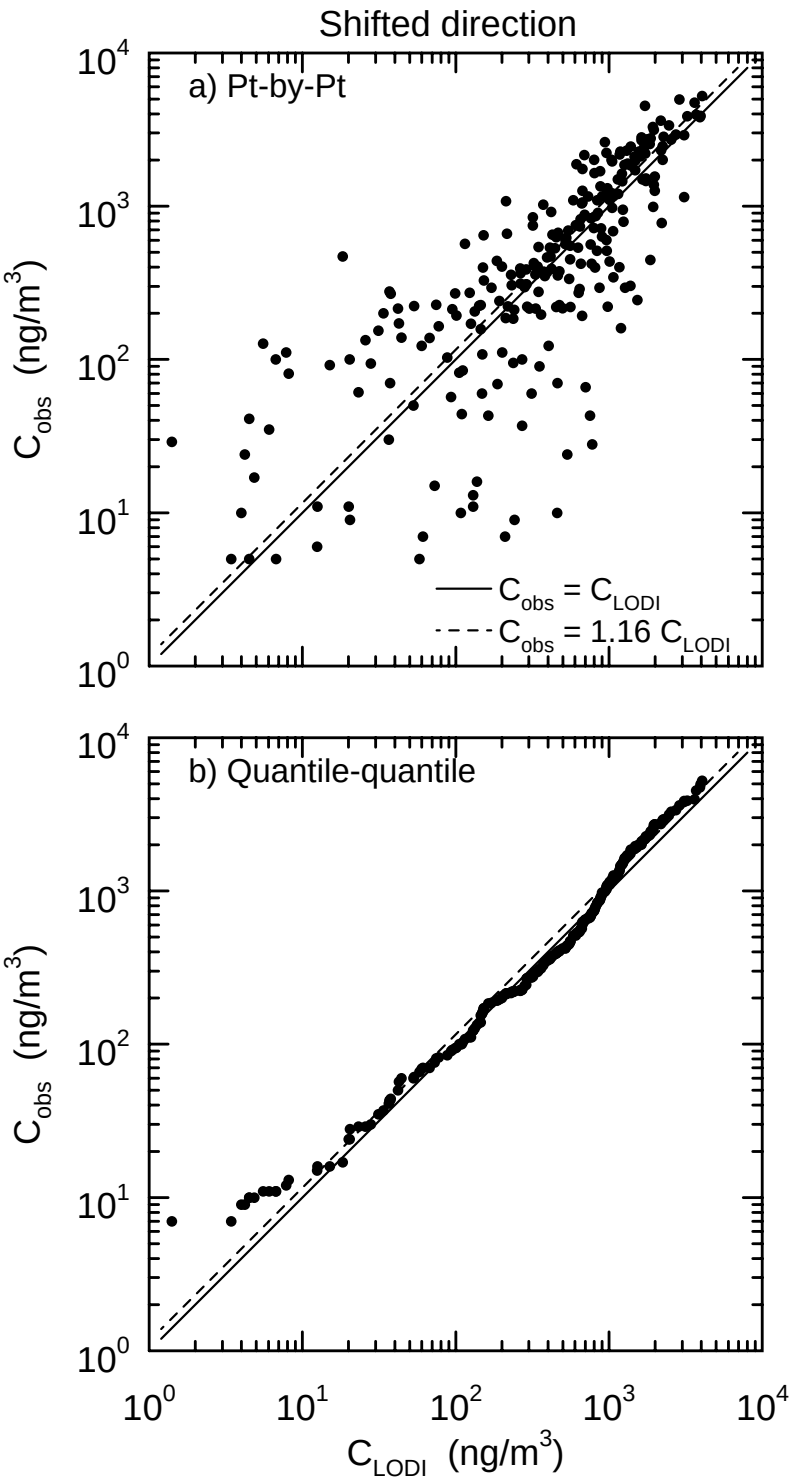

Figure 12: Observed 1-h values versus LODI predictions of ground-level concentrations in the Copenhagen experiment: a) point-by-point comparison, and b) quantile-quantile comparison; only nonzero concentrations included. Dashed line corresonds to geometric mean (0.86) of C_{LODI}/C_{obs}, where the geometric standard deviation of the ratio is 4. LODI wind direction shifted to equal observed direction.

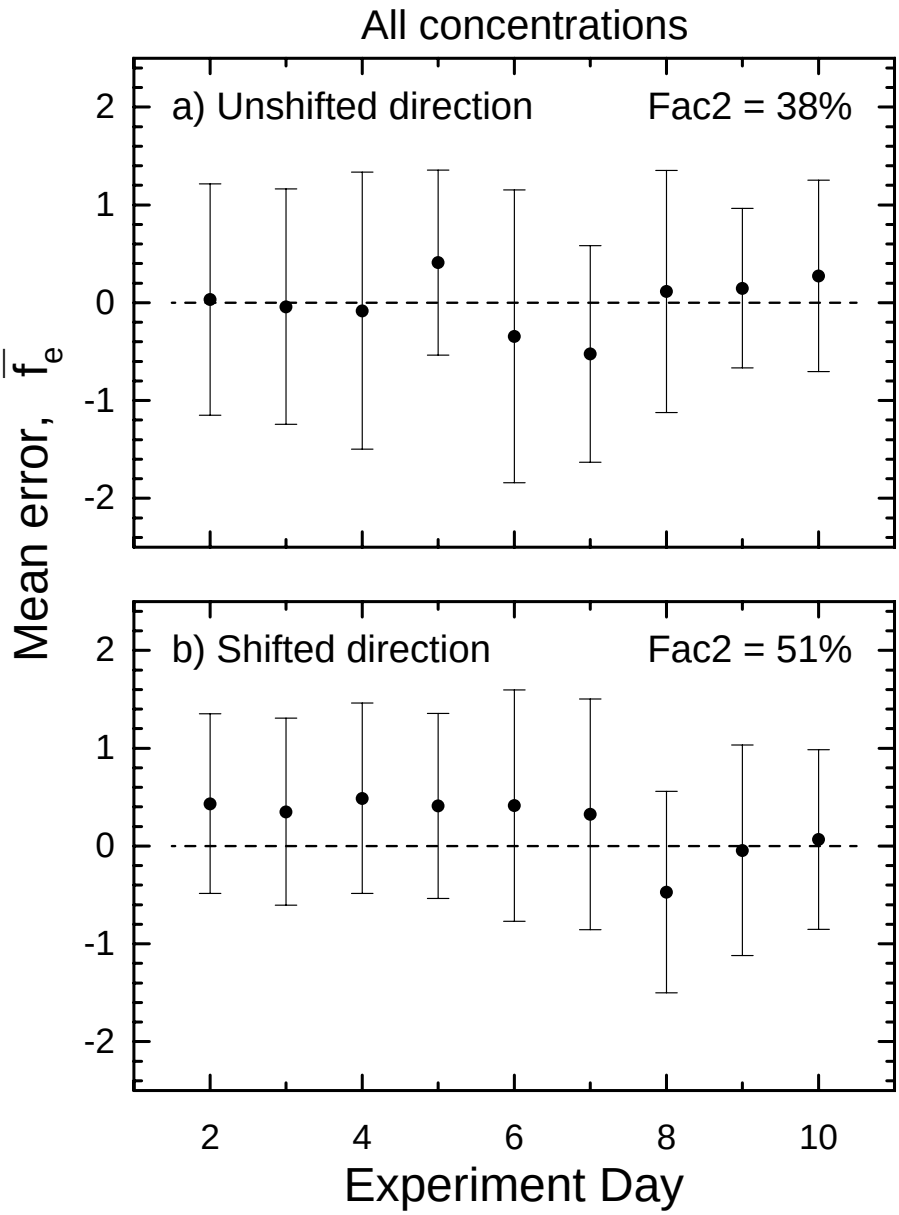

Figure 13: Mean fractional error between LODI predictions and observed concentrations over all monitors as a function of experiment day for the a) unshifted (LODI) wind direction, and b) shifted direction. Errors bars correspond to ± one standard deviation in the f_e values, dashed line to the ideal $\overline{f_e}$ (= 0), and $Fac2$ is the percent of predictions within a factor of 2 of the observations.

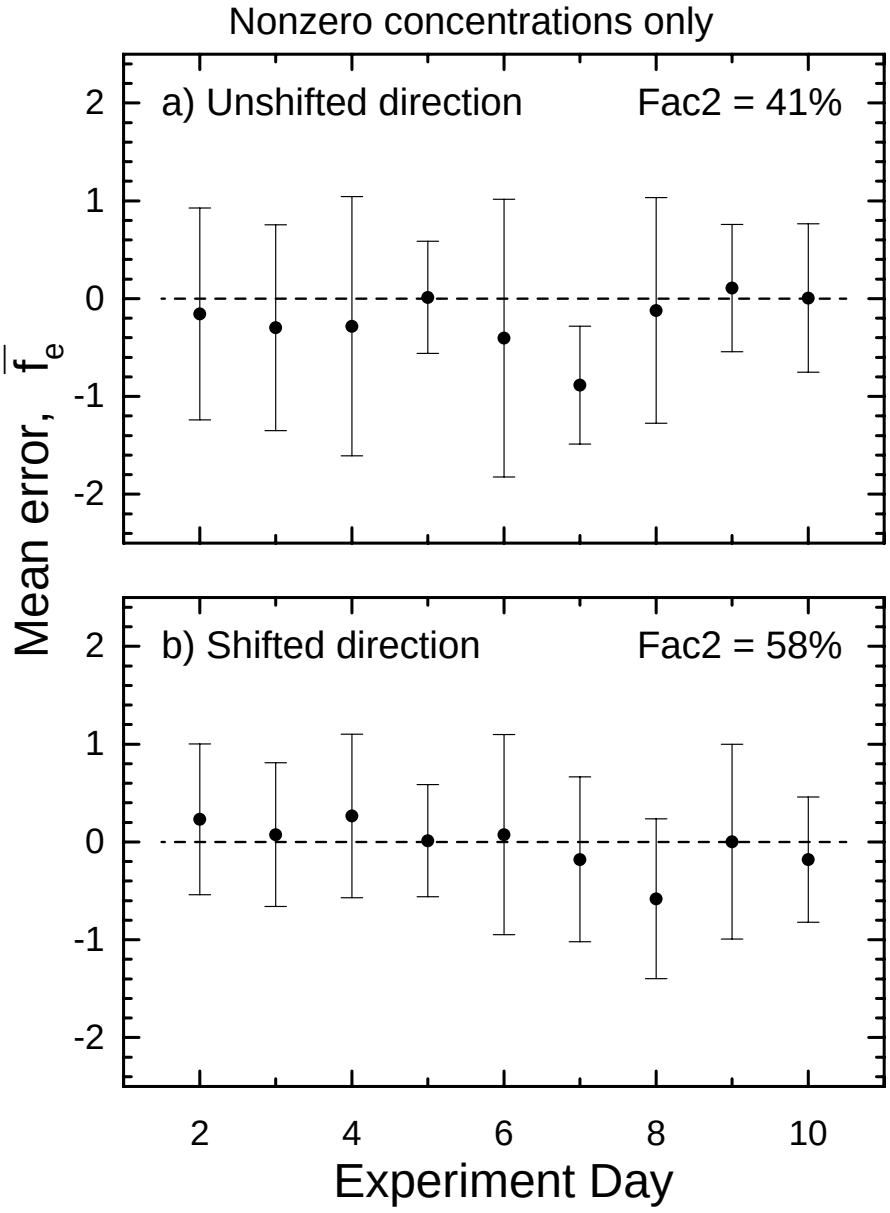

Figure 14: Same as Fig. 13 but for nonzero concentrations only.

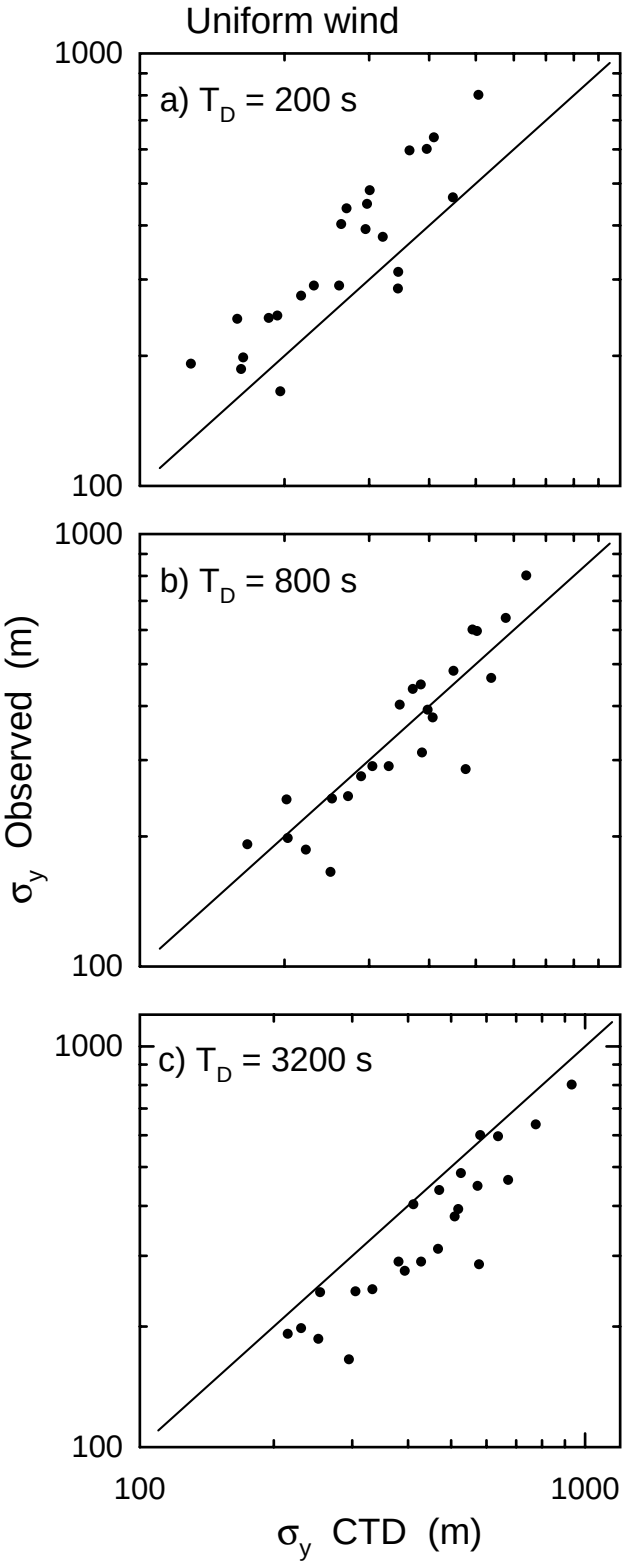

Figure 15: Comparison between observed and predicted 1-h σ_y values for a uniform wind and three values of T_D in a constant T_D approach, $\sigma_{y\ CTD}$.

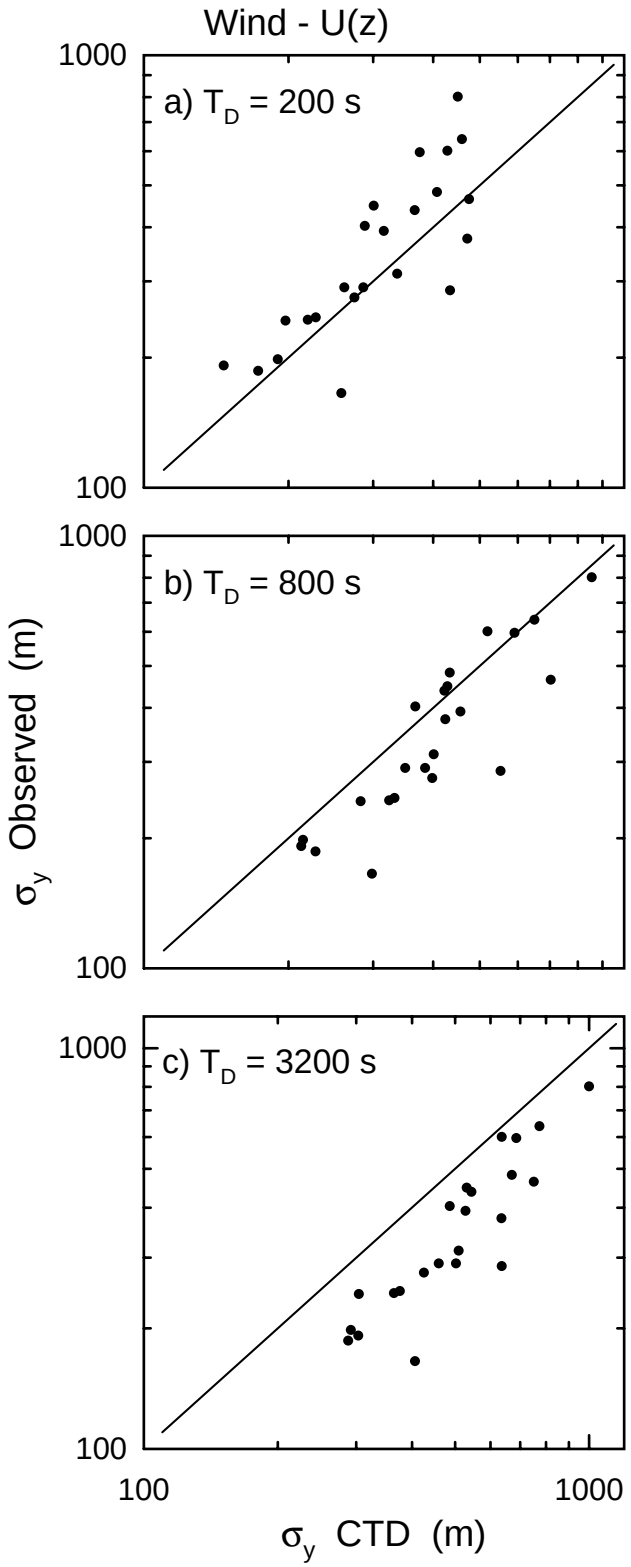

Figure 16: Same as Fig. 15 but for height-dependent wind profile.

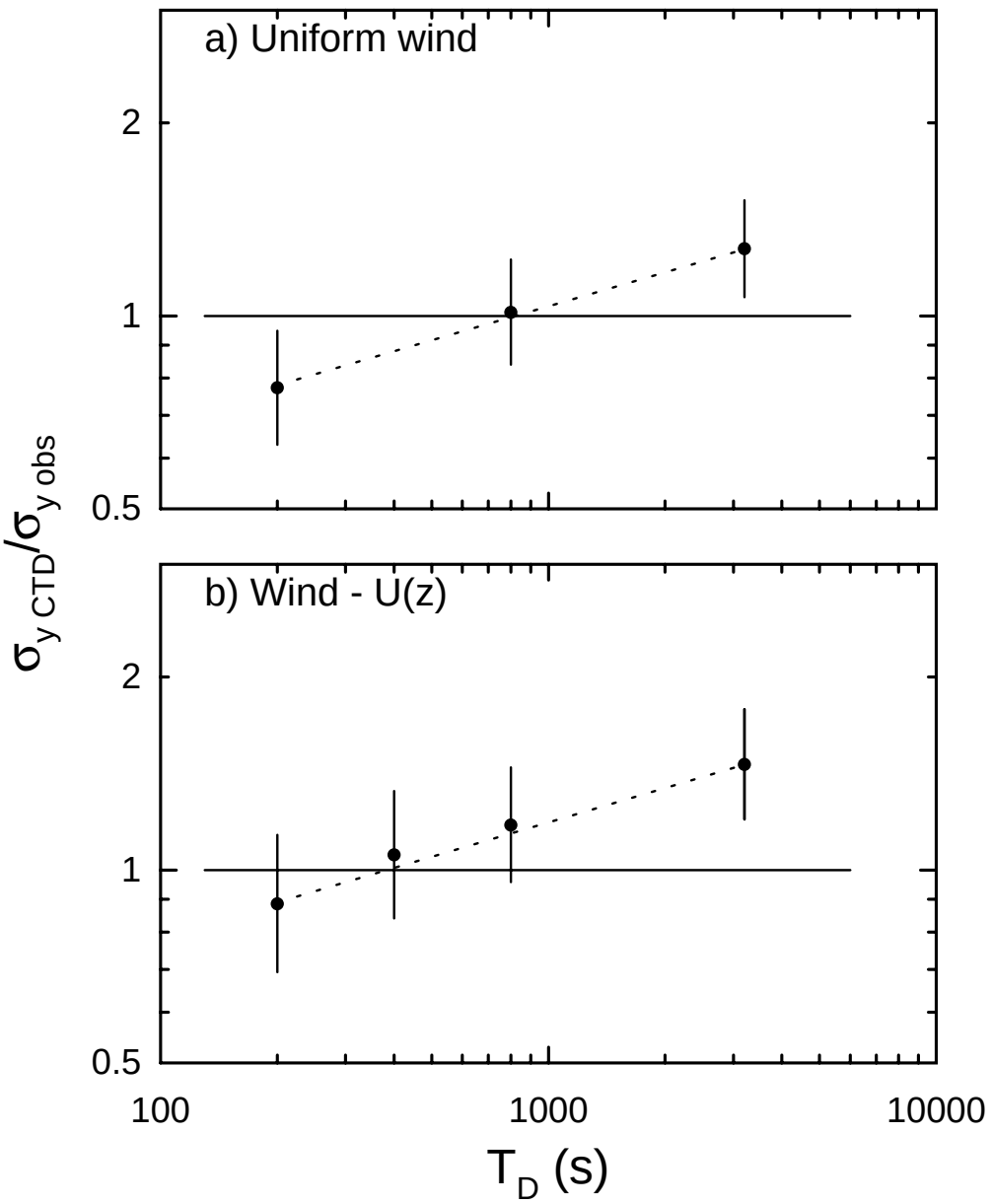

Figure 17: Geometric mean of ratio of predicted-to-observed σ_y (points) as a function of T_D for σ_y predictions with a constant T_D and either uniform or height-dependent winds; geometric standard deviation shown by vertical lines and ideal value of ratio shown by horizontal line.